

Chapter 9 / Failure



An oil tanker that fractured in a brittle manner by crack propagation around its girth. (Photography by Neal Boenzi. Reprinted with permission from *The New York Times*.)

Why Study Failure?

The design of a component or structure often calls upon the engineer to minimize the possibility of failure. Thus, it is important to understand the mechanics of the various failure modes—i.e., fracture, fatigue, and creep—and, in addition, be familiar with

appropriate design principles that may be employed to prevent in-service failures. {For example, we discuss in Section 20.5 material selection and processing issues relating to the fatigue of an automobile valve spring.}

Learning Objectives

After studying this chapter you should be able to do the following:

1. Describe the mechanism of crack propagation for both ductile and brittle modes of fracture.
2. Explain why the strengths of brittle materials are much lower than predicted by theoretical calculations.
3. Define fracture toughness in terms of (a) a brief statement, and (b) an equation; define all parameters in this equation.
- {4. Make distinctions between *stress intensity factor*, *fracture toughness*, and *plane strain fracture toughness*.}
5. Briefly explain why there is normally significant scatter in the fracture strength for identical specimens of the same ceramic material.
6. Briefly describe the phenomenon of *crazing*.
7. Name and describe the two impact fracture testing techniques.
8. Define fatigue and specify the conditions under which it occurs.
9. From a fatigue plot for some material, determine (a) the fatigue lifetime (at a specified stress level), and (b) the fatigue strength (at a specified number of cycles).
10. Define creep and specify the conditions under which it occurs.
11. Given a creep plot for some material, determine (a) the steady-state creep rate, and (b) the rupture lifetime.

9.1 INTRODUCTION

The failure of engineering materials is almost always an undesirable event for several reasons; these include human lives that are put in jeopardy, economic losses, and the interference with the availability of products and services. Even though the causes of failure and the behavior of materials may be known, prevention of failures is difficult to guarantee. The usual causes are improper materials selection and processing and inadequate design of the component or its misuse. It is the responsibility of the engineer to anticipate and plan for possible failure and, in the event that failure does occur, to assess its cause and then take appropriate preventive measures against future incidents.

Topics to be addressed in this chapter are the following: simple fracture (both ductile and brittle modes), fundamentals of fracture mechanics, impact fracture testing, the ductile-to-brittle transition, fatigue, and creep. These discussions include failure mechanisms, testing techniques, and methods by which failure may be prevented or controlled.

FRACTURE

9.2 FUNDAMENTALS OF FRACTURE

Simple fracture is the separation of a body into two or more pieces in response to an imposed stress that is static (i.e., constant or slowly changing with time) and at temperatures that are low relative to the melting temperature of the material. The applied stress may be tensile, compressive, shear, or torsional; the present discussion will be confined to fractures that result from uniaxial tensile loads. For engineering materials, two fracture modes are possible: **ductile** and **brittle**. Classification is based on the ability of a material to experience plastic deformation. Ductile materials typically exhibit substantial plastic deformation with high energy absorption before fracture. On the other hand, there is normally little or no plastic deformation with low energy absorption accompanying a brittle fracture. The tensile stress-strain behaviors of both fracture types may be reviewed in Figure 7.13.

“Ductile” and “brittle” are relative terms; whether a particular fracture is one mode or the other depends on the situation. Ductility may be quantified in terms

of percent elongation (Equation 7.11) and percent reduction in area (Equation 7.12). Furthermore, ductility is a function of temperature of the material, the strain rate, and the stress state. The disposition of normally ductile materials to fail in a brittle manner is discussed in Section 9.8.

Any fracture process involves two steps—crack formation and propagation—in response to an imposed stress. The mode of fracture is highly dependent on the mechanism of crack propagation. Ductile fracture is characterized by extensive plastic deformation in the vicinity of an advancing crack. Furthermore, the process proceeds relatively slowly as the crack length is extended. Such a crack is often said to be *stable*. That is, it resists any further extension unless there is an increase in the applied stress. In addition, there will ordinarily be evidence of appreciable gross deformation at the fracture surfaces (e.g., twisting and tearing). On the other hand, for brittle fracture, cracks may spread extremely rapidly, with very little accompanying plastic deformation. Such cracks may be said to be *unstable*, and crack propagation, once started, will continue spontaneously without an increase in magnitude of the applied stress.

Ductile fracture is almost always preferred for two reasons. First, brittle fracture occurs suddenly and catastrophically without any warning; this is a consequence of the spontaneous and rapid crack propagation. On the other hand, for ductile fracture, the presence of plastic deformation gives warning that fracture is imminent, allowing preventive measures to be taken. Second, more strain energy is required to induce ductile fracture inasmuch as ductile materials are generally tougher. Under the action of an applied tensile stress, most metal alloys are ductile, whereas ceramics are notably brittle, and polymers may exhibit both types of fracture.

9.3 DUCTILE FRACTURE

Ductile fracture surfaces will have their own distinctive features on both macroscopic and microscopic levels. Figure 9.1 shows schematic representations for two characteristic macroscopic fracture profiles. The configuration shown in Figure 9.1a is found for extremely soft metals, such as pure gold and lead at room temperature, and other metals, polymers, and inorganic glasses at elevated temperatures. These highly ductile materials neck down to a point fracture, showing virtually 100% reduction in area.

The most common type of tensile fracture profile for ductile metals is that represented in Figure 9.1b, which fracture is preceded by only a moderate amount

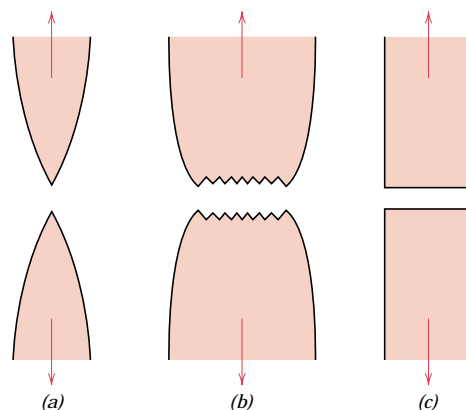


FIGURE 9.1 (a) Highly ductile fracture in which the specimen necks down to a point. (b) Moderately ductile fracture after some necking. (c) Brittle fracture without any plastic deformation.

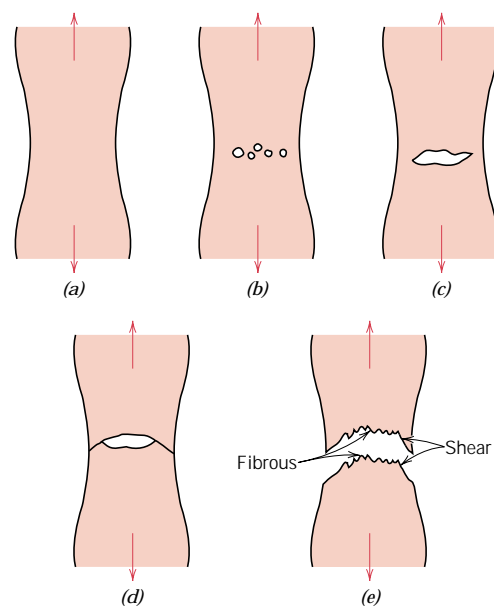


FIGURE 9.2 Stages in the cup-and-cone fracture. (a) Initial necking. (b) Small cavity formation. (c) Coalescence of cavities to form a crack. (d) Crack propagation. (e) Final shear fracture at a 45° angle relative to the tensile direction. (From K. M. Ralls, T. H. Courtney, and J. Wulff, *Introduction to Materials Science and Engineering*, p. 468. Copyright © 1976 by John Wiley & Sons, New York. Reprinted by permission of John Wiley & Sons, Inc.)

of necking. The fracture process normally occurs in several stages (Figure 9.2). First, after necking begins, small cavities, or microvoids, form in the interior of the cross section, as indicated in Figure 9.2*b*. Next, as deformation continues, these microvoids enlarge, come together, and coalesce to form an elliptical crack, which has its long axis perpendicular to the stress direction. The crack continues to grow in a direction parallel to its major axis by this microvoid coalescence process (Figure 9.2*c*). Finally, fracture ensues by the rapid propagation of a crack around the outer perimeter of the neck (Figure 9.2*d*), by shear deformation at an angle of about 45° with the tensile axis—this is the angle at which the shear stress is a maximum. Sometimes a fracture having this characteristic surface contour is termed a *cup-and-cone fracture* because one of the mating surfaces is in the form of a cup, the other like a cone. In this type of fractured specimen (Figure 9.3*a*), the central

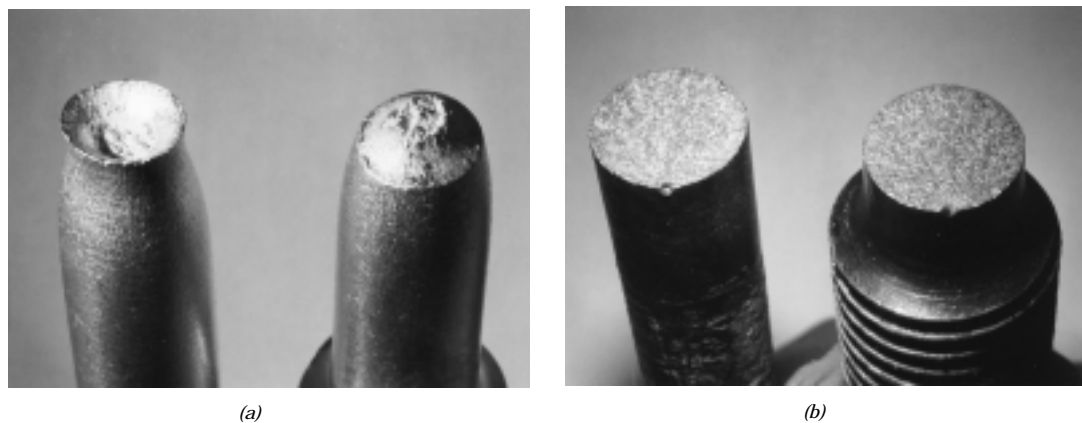


FIGURE 9.3 (a) Cup-and-cone fracture in aluminum. (b) Brittle fracture in a mild steel.

interior region of the surface has an irregular and fibrous appearance, which is indicative of plastic deformation.

FRACTOGRAPHIC STUDIES (CD-ROM)

9.4 BRITTLE FRACTURE

Brittle fracture takes place without any appreciable deformation, and by rapid crack propagation. The direction of crack motion is very nearly perpendicular to the direction of the applied tensile stress and yields a relatively flat fracture surface, as indicated in Figure 9.1c.

Fracture surfaces of materials that failed in a brittle manner will have their own distinctive patterns; any signs of gross plastic deformation will be absent. For example, in some steel pieces, a series of V-shaped “chevron” markings may form near the center of the fracture cross section that point back toward the crack initiation site (Figure 9.5a). Other brittle fracture surfaces contain lines or ridges that radiate from the origin of the crack in a fanlike pattern (Figure 9.5b). Often, both of these marking patterns will be sufficiently coarse to be discerned with the naked eye. For very hard and fine-grained metals, there will be no discernible fracture pattern. Brittle fracture in amorphous materials, such as ceramic glasses, yields a relatively shiny and smooth surface.

For most brittle crystalline materials, crack propagation corresponds to the successive and repeated breaking of atomic bonds along specific crystallographic planes; such a process is termed *cleavage*. This type of fracture is said to be **transgranular** (or *transcrystalline*), because the fracture cracks pass through the grains. Macroscopically, the fracture surface may have a grainy or faceted texture (Figure 9.3b), as a result of changes in orientation of the cleavage planes from grain to grain. This feature is more evident in the scanning electron micrograph shown in Figure 9.6a.

In some alloys, crack propagation is along grain boundaries; this fracture is termed **intergranular**. Figure 9.6b is a scanning electron micrograph showing a typical intergranular fracture, in which the three-dimensional nature of the grains may be seen. This type of fracture normally results subsequent to the occurrence of processes that weaken or embrittle grain boundary regions.

9.5a PRINCIPLES OF FRACTURE MECHANICS [DETAILED VERSION (CD-ROM)]

9.5b PRINCIPLES OF FRACTURE MECHANICS (CONCISE VERSION)

Brittle fracture of normally ductile materials, such as that shown in the chapter-opening photograph of this chapter, has demonstrated the need for a better understanding of the mechanisms of fracture. Extensive research endeavors over the past several decades have led to the evolution of the field of **fracture mechanics**. This subject allows quantification of the relationships between material properties, stress level, the presence of crack-producing flaws, and crack propagation mechanisms. Design engineers are now better equipped to anticipate, and thus prevent, structural failures. The present discussion centers on some of the fundamental principles of the mechanics of fracture.

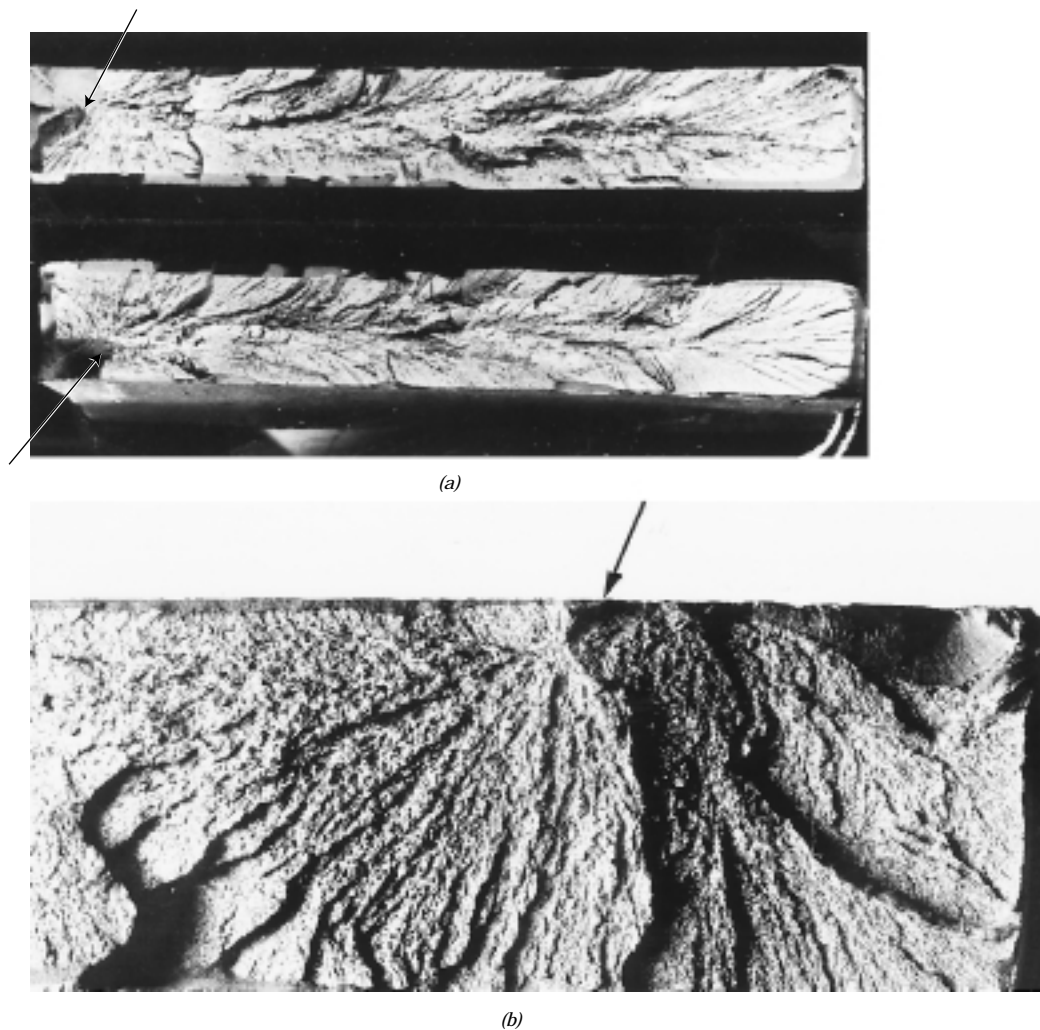
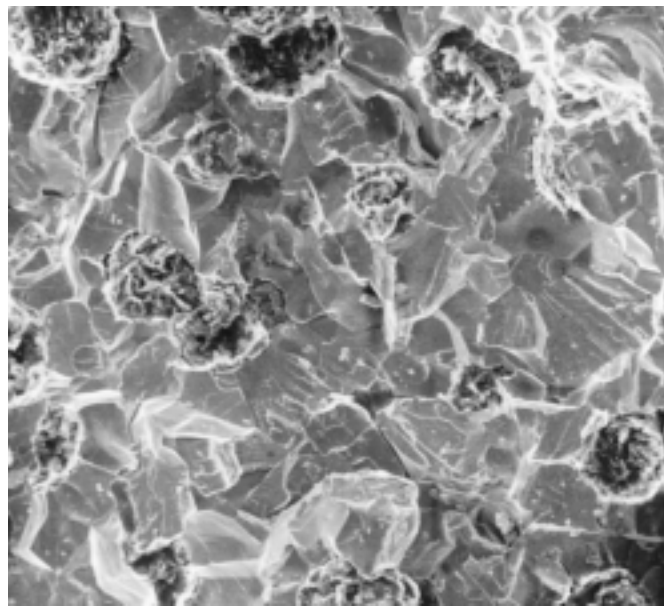


FIGURE 9.5 (a) Photograph showing V-shaped “chevron” markings characteristic of brittle fracture. Arrows indicate origin of crack. Approximately actual size. (From R. W. Hertzberg, *Deformation and Fracture Mechanics of Engineering Materials*, 3rd edition. Copyright © 1989 by John Wiley & Sons, New York. Reprinted by permission of John Wiley & Sons, Inc. Photograph courtesy of Roger Slutter, Lehigh University.) (b) Photograph of a brittle fracture surface showing radial fan-shaped ridges. Arrow indicates origin of crack. Approximately 2×. (Reproduced with permission from D. J. Wulpi, *Understanding How Components Fail*, American Society for Metals, Materials Park, OH, 1985.)

STRESS CONCENTRATION

The measured fracture strengths for most brittle materials are significantly lower than those predicted by theoretical calculations based on atomic bonding energies. This discrepancy is explained by the presence of very small, microscopic flaws or cracks that always exist under normal conditions at the surface and within the interior of a body of material. These flaws are a detriment to the fracture strength because an applied stress may be amplified or concentrated at the tip, the magnitude



(a)



(b)

FIGURE 9.6 (a) Scanning electron fractograph of ductile cast iron showing a transgranular fracture surface. Magnification unknown. (From V. J. Colangelo and F. A. Heiser, *Analysis of Metallurgical Failures*, 2nd edition. Copyright © 1987 by John Wiley & Sons, New York. Reprinted by permission of John Wiley & Sons, Inc.) (b) Scanning electron fractograph showing an intergranular fracture surface. 50 \times . (Reproduced with permission from *ASM Handbook*, Vol. 12, *Fractography*, ASM International, Materials Park, OH, 1987.)

of this amplification depending on crack orientation and geometry. This phenomenon is demonstrated in Figure 9.7, a stress profile across a cross section containing an internal crack. As indicated by this profile, the magnitude of this localized stress diminishes with distance away from the crack tip. At positions far removed, the stress is just the nominal stress σ_0 , or the load divided by the specimen cross-

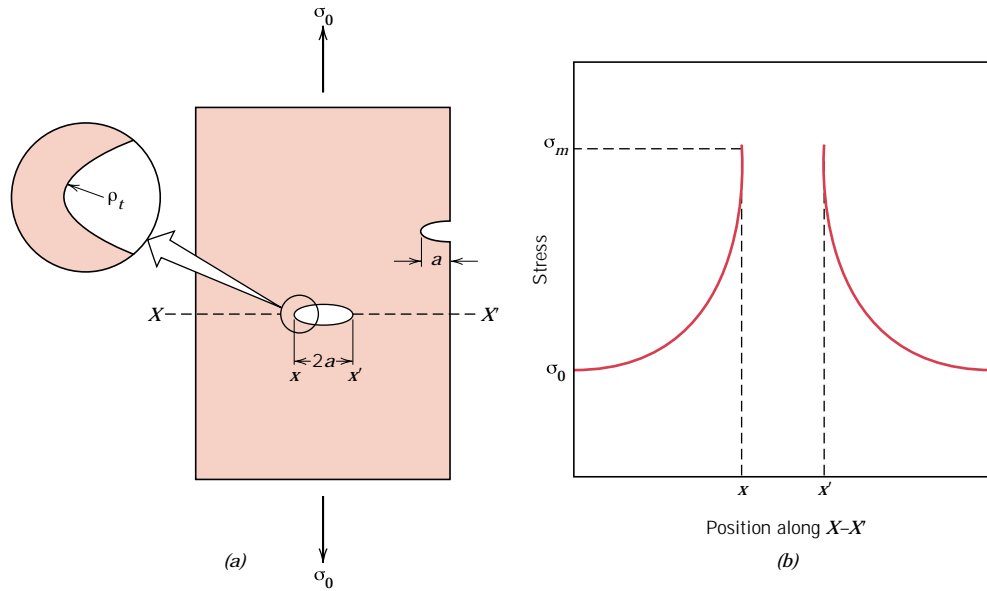


FIGURE 9.7 (a) The geometry of surface and internal cracks. (b) Schematic stress profile along the line $X-X'$ in (a), demonstrating stress amplification at crack tip positions.

sectional area (perpendicular to this load). Due to their ability to amplify an applied stress in their locale, these flaws are sometimes called **stress raisers**.

If it is assumed that a crack has an elliptical shape and is oriented perpendicular to the applied stress, the maximum stress at the crack tip, σ_m , may be approximated by

$$\sigma_m = 2\sigma_0 \left(\frac{a}{\rho_t} \right)^{1/2} \quad (9.1b)$$

where σ_0 is the magnitude of the nominal applied tensile stress, ρ_t is the radius of curvature of the crack tip (Figure 9.7a), and a represents the length of a surface crack, or half of the length of an internal crack. For a relatively long microcrack that has a small tip radius of curvature, the factor $(a/\rho_t)^{1/2}$ may be very large. This will yield a value of σ_m that is many times the value of σ_0 .

Sometimes the ratio σ_m/σ_0 is denoted as the *stress concentration factor* K_t :

$$K_t = \frac{\sigma_m}{\sigma_0} = 2 \left(\frac{a}{\rho_t} \right)^{1/2} \quad (9.2)$$

which is simply a measure of the degree to which an external stress is amplified at the tip of a crack.

By way of comment, it should be said that stress amplification is not restricted to these microscopic defects; it may occur at macroscopic internal discontinuities (e.g., voids), at sharp corners, and at notches in large structures.

Furthermore, the effect of a stress raiser is more significant in brittle than in ductile materials. For a ductile material, plastic deformation ensues when the

maximum stress exceeds the yield strength. This leads to a more uniform distribution of stress in the vicinity of the stress raiser and to the development of a maximum stress concentration factor less than the theoretical value. Such yielding and stress redistribution do not occur to any appreciable extent around flaws and discontinuities in brittle materials; therefore, essentially the theoretical stress concentration will result.

Using principles of fracture mechanics, it is possible to show that the critical stress σ_c required for crack propagation in a brittle material is described by the expression

$$\sigma_c = \left(\frac{2E\gamma_s}{\pi a} \right)^{1/2} \quad (9.3)$$

where

E = modulus of elasticity

γ_s = specific surface energy

a = one half the length of an internal crack

All brittle materials contain a population of small cracks and flaws that have a variety of sizes, geometries, and orientations. When the magnitude of a tensile stress at the tip of one of these flaws exceeds the value of this critical stress, a crack forms and then propagates, which results in fracture. Very small and virtually defect-free metallic and ceramic whiskers have been grown with fracture strengths that approach their theoretical values.

EXAMPLE PROBLEM 9.1

A relatively large plate of a glass is subjected to a tensile stress of 40 MPa. If the specific surface energy and modulus of elasticity for this glass are 0.3 J/m² and 69 GPa, respectively, determine the maximum length of a surface flaw that is possible without fracture.

SOLUTION

To solve this problem it is necessary to employ Equation 9.3. Rearrangement of this expression such that a is the dependent variable, and realizing that $\sigma = 40$ MPa, $\gamma_s = 0.3$ J/m², and $E = 69$ GPa leads to

$$\begin{aligned} a &= \frac{2E\gamma_s}{\pi\sigma^2} \\ &= \frac{(2)(69 \times 10^9 \text{ N/m}^2)(0.3 \text{ N/m})}{\pi(40 \times 10^6 \text{ N/m}^2)^2} \\ &= 8.2 \times 10^{-6} \text{ m} = 0.0082 \text{ mm} = 8.2 \mu\text{m} \end{aligned}$$

FRACTURE TOUGHNESS

Furthermore, using fracture mechanical principles, an expression has been developed that relates this critical stress for crack propagation (σ_c) to crack length (a) as

$$K_c = Y\sigma_c\sqrt{\pi a} \quad (9.9a)$$

In this expression K_c is the **fracture toughness**, a property that is a measure of a material's resistance to brittle fracture when a crack is present. Worth noting is that K_c has the unusual units of $\text{MPa}\sqrt{\text{m}}$ or $\text{psi}\sqrt{\text{in.}}$ (alternatively $\text{ksi}\sqrt{\text{in.}}$). Furthermore, Y is a dimensionless parameter or function that depends on both crack and specimen sizes and geometries, as well as the manner of load application.

Relative to this Y parameter, for planar specimens containing cracks that are much shorter than the specimen width, Y has a value of approximately unity. For example, for a plate of infinite width having a through-thickness crack (Figure 9.11a), $Y = 1.0$; whereas for a plate of semi-infinite width containing an edge crack of length a (Figure 9.11b), $Y \cong 1.1$. Mathematical expressions for Y have been determined for a variety of crack-specimen geometries; these expressions are often relatively complex.

For relatively thin specimens, the value of K_c will depend on specimen thickness. However, when specimen thickness is much greater than the crack dimensions, K_c becomes independent of thickness; under these conditions a condition of **plane strain** exists. By plane strain we mean that when a load operates on a crack in the manner represented in Figure 9.11a, there is no strain component perpendicular to the front and back faces. The K_c value for this thick-specimen situation is known as the **plane strain fracture toughness** K_{Ic} ; furthermore, it is also defined by

$$K_{Ic} = Y\sigma\sqrt{\pi a} \quad (9.11)$$

K_{Ic} is the fracture toughness cited for most situations. The *I* (i.e., Roman numeral “one”) subscript for K_{Ic} denotes that the plane strain fracture toughness is for mode I crack displacement, as illustrated in Figure 9.9a⁵ (see page 244).

Brittle materials, for which appreciable plastic deformation is not possible in front of an advancing crack, have low K_{Ic} values and are vulnerable to catastrophic failure. On the other hand, K_{Ic} values are relatively large for ductile materials. Fracture mechanics is especially useful in predicting catastrophic failure in materials

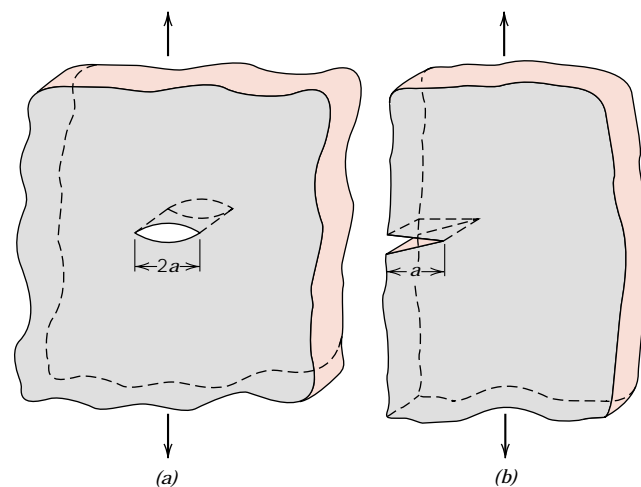
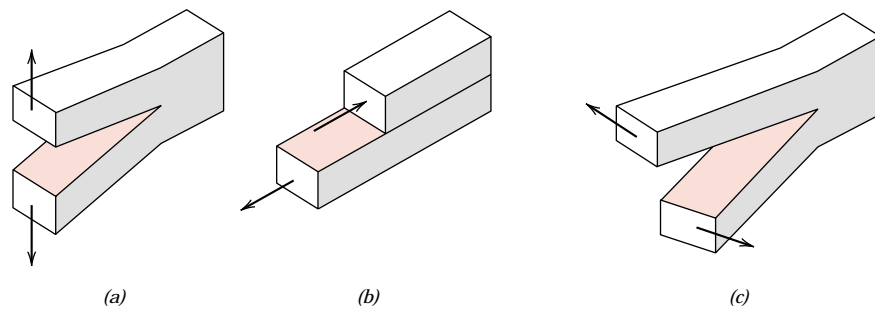


FIGURE 9.11 Schematic representations of (a) an interior crack in a plate of infinite width, and (b) an edge crack in a plate of semi-infinite width.

⁵ Two other crack displacement modes denoted by II and III and as illustrated in Figures 9.9b and 9.9c are also possible; however, mode I is most commonly encountered.

FIGURE 9.9 The three modes of crack surface displacement. (a) Mode I, opening or tensile mode; (b) mode II, sliding mode; and (c) mode III, tearing mode.



having intermediate ductilities. Plane strain fracture toughness values for a number of different materials are presented in Table 9.1; a more extensive list of K_{Ic} values is contained in Table B.5, Appendix B.

The plane strain fracture toughness K_{Ic} is a fundamental material property that depends on many factors, the most influential of which are temperature, strain rate, and microstructure. The magnitude of K_{Ic} diminishes with increasing strain rate and

Table 9.1 Room-Temperature Yield Strength and Plane Strain Fracture Toughness Data for Selected Engineering Materials

| Material | Yield Strength | | K_{Ic} | |
|---|----------------|----------|----------------|------------------|
| | MPa | ksi | MPa \sqrt{m} | ksi $\sqrt{in.}$ |
| Metals | | | | |
| Aluminum Alloy ^a (7075-T651) | 495 | 72 | 24 | 22 |
| Aluminum Alloy ^a (2024-T3) | 345 | 50 | 44 | 40 |
| Titanium Alloy ^a (Ti-6Al-4V) | 910 | 132 | 55 | 50 |
| Alloy Steel ^a (4340 tempered @ 260°C) | 1640 | 238 | 50.0 | 45.8 |
| Alloy Steel ^a (4340 tempered @ 425°C) | 1420 | 206 | 87.4 | 80.0 |
| Ceramics | | | | |
| Concrete | — | — | 0.2–1.4 | 0.18–1.27 |
| Soda-Lime Glass | — | — | 0.7–0.8 | 0.64–0.73 |
| Aluminum Oxide | — | — | 2.7–5.0 | 2.5–4.6 |
| Polymers | | | | |
| Polystyrene (PS) | — | — | 0.7–1.1 | 0.64–1.0 |
| Polymethyl Methacrylate (PMMA) | 53.8–73.1 | 7.8–10.6 | 0.7–1.6 | 0.64–1.5 |
| Polycarbonate (PC) | 62.1 | 9.0 | 2.2 | 2.0 |

^a **Source:** Reprinted with permission, *Advanced Materials and Processes*, ASM International, © 1990.

decreasing temperature. Furthermore, an enhancement in yield strength wrought by solid solution or dispersion additions or by strain hardening generally produces a corresponding decrease in K_{Ic} . Furthermore, K_{Ic} normally increases with reduction in grain size as composition and other microstructural variables are maintained constant. Yield strengths are included for some of the materials listed in Table 9.1. Furthermore, K_{Ic} normally increases with reduction in grain size as composition and other microstructural variables are maintained constant.

Several different testing techniques are used to measure K_{Ic} .⁶ Virtually any specimen size and shape consistent with mode I crack displacement may be utilized, and accurate values will be realized provided that the Y scale parameter in Equation 9.11 has been properly determined.

DESIGN USING FRACTURE MECHANICS

According to Equations 9.9a and 9.11, three variables must be considered relative to the possibility for fracture of some structural component—viz. the fracture toughness (K_c) or plane strain fracture toughness (K_{Ic}), the imposed stress (σ), and the flaw size (a), assuming, of course, that Y has been determined. When designing a component, it is first important to decide which of these variables are constrained by the application and which are subject to design control. For example, material selection (and hence K_c or K_{Ic}) is often dictated by factors such as density (for lightweight applications) or the corrosion characteristics of the environment. Or, the allowable flaw size is either measured or specified by the limitations of available flaw detection techniques. It is important to realize, however, that once any combination of two of the above parameters is prescribed, the third becomes fixed (Equations 9.9a and 9.11). For example, assume that K_{Ic} and the magnitude of a are specified by application constraints; therefore, the design (or critical) stress σ_c must be

$$\sigma_c \leq \frac{K_{Ic}}{Y\sqrt{\pi a}} \quad (9.13)$$

On the other hand, if stress level and plane strain fracture toughness are fixed by the design situation, then the maximum allowable flaw size a_c is

$$a_c = \frac{1}{\pi} \left(\frac{K_{Ic}}{\sigma Y} \right)^2 \quad (9.14)$$

A number of nondestructive test (NDT) techniques have been developed that permit detection and measurement of both internal and surface flaws. Such NDT methods are used to avoid the occurrence of catastrophic failure by examining structural components for defects and flaws that have dimensions approaching the critical size.



DESIGN EXAMPLE 9.1

Consider the thin-walled spherical tank of radius r and thickness t (Figure 9.15) that may be used as a pressure vessel.

⁶ See for example ASTM Standard E 399, “Standard Test Method for Plane Strain Fracture Toughness of Metallic Materials.”

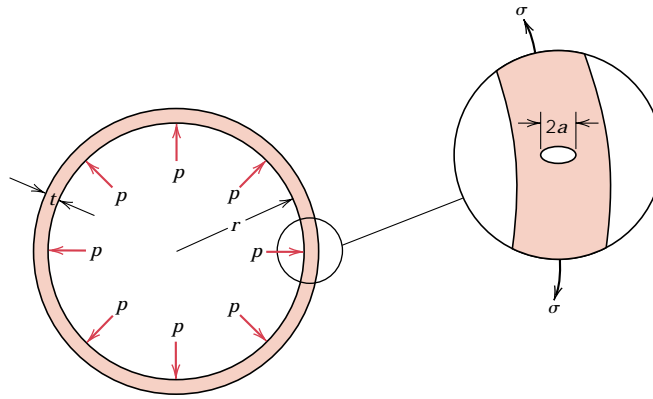


FIGURE 9.15 Schematic diagram showing the cross section of a spherical tank that is subjected to an internal pressure p , and that has a radial crack of length $2a$ in its wall.

(a) One design of such a tank calls for yielding of the wall material prior to failure as a result of the formation of a crack of critical size and its subsequent rapid propagation. Thus, plastic distortion of the wall may be observed and the pressure within the tank released before the occurrence of catastrophic failure. Consequently, materials having large critical crack lengths are desired. On the basis of this criterion, rank the metal alloys listed in Table B.5, Appendix B, as to critical crack size, from longest to shortest.

(b) An alternative design that is also often utilized with pressure vessels is termed *leak-before-break*. Using principles of fracture mechanics, allowance is made for the growth of a crack through the thickness of the vessel wall prior to the occurrence of rapid crack propagation (Figure 9.15). Thus, the crack will completely penetrate the wall without catastrophic failure, allowing for its detection by the leaking of pressurized fluid. With this criterion the critical crack length a_c (i.e., one-half of the total internal crack length) is taken to be equal to the pressure vessel thickness t . Allowance for $a_c = t$ instead of $a_c = t/2$ assures that fluid leakage will occur prior to the buildup of dangerously high pressures. Using this criterion, rank the metal alloys in Table B.5, Appendix B as to the maximum allowable pressure.

For this spherical pressure vessel, the circumferential wall stress σ is a function of the pressure p in the vessel and the radius r and wall thickness t according to

$$\sigma = \frac{pr}{2t} \tag{9.15}$$

For both parts (a) and (b) assume a condition of plane strain.

SOLUTION

(a) For the first design criterion, it is desired that the circumferential wall stress be less than the yield strength of the material. Substitution of σ_y for σ in Equation 9.11, and incorporation of a factor of safety N leads to

$$K_{Ic} = Y \left(\frac{\sigma_y}{N} \right) \sqrt{\pi a_c} \tag{9.16}$$

where a_c is the critical crack length. Solving for a_c yields the following expression:

$$a_c = \frac{N^2}{Y^2 \pi} \left(\frac{K_{Ic}}{\sigma_y} \right)^2 \tag{9.17}$$

Table 9.2 Ranking of Several Metal Alloys Relative to Critical Crack Length (Yielding Criterion) for a Thin-Walled Spherical Pressure Vessel

| <i>Material</i> | $\left(\frac{K_{Ic}}{\sigma_y}\right)^2$ (mm) |
|----------------------------------|---|
| Medium carbon (1040) steel | 43.1 |
| AZ31B magnesium | 19.6 |
| 2024 aluminum (T3) | 16.3 |
| Ti-5Al-2.5Sn titanium | 6.6 |
| 4140 steel (tempered @ 482°C) | 5.3 |
| 4340 steel (tempered @ 425°C) | 3.8 |
| Ti-6Al-4V titanium | 3.7 |
| 17-7PH steel | 3.4 |
| 7075 aluminum (T651) | 2.4 |
| 4140 steel (tempered @ 370°C) | 1.6 |
| 4340 Steel (tempered @ 260°C) | 0.93 |

Therefore, the critical crack length is proportional to the square of the K_{Ic}/σ_y ratio, which is the basis for the ranking of the metal alloys in Table B.5. The ranking is provided in Table 9.2, where it may be seen that the medium carbon (1040) steel with the largest ratio has the longest critical crack length, and, therefore, is the most desirable material on the basis of this criterion.

(b) As stated previously, the leak-before-break criterion is just met when one-half of the internal crack length is equal to the thickness of the pressure vessel—i.e., when $a = t$. Substitution of $a = t$ into Equation 9.11 gives

$$K_{Ic} = Y\sigma\sqrt{\pi t} \quad (9.18)$$

And, from Equation 9.15

$$t = \frac{pr}{2\sigma} \quad (9.19)$$

The stress is replaced by the yield strength, inasmuch as the tank should be designed to contain the pressure without yielding; furthermore, substitution of Equation 9.19 into Equation 9.18, after some rearrangement, yields the following expression:

$$p = \frac{2}{Y^2\pi r} \left(\frac{K_{Ic}^2}{\sigma_y}\right) \quad (9.20)$$

Hence, for some given spherical vessel of radius r , the maximum allowable pressure consistent with this leak-before-break criterion is proportional to K_{Ic}^2/σ_y . The same several materials are ranked according to this ratio in Table 9.3; as may be noted, the medium carbon steel will contain the greatest pressures.

Of the eleven metal alloys that are listed in Table B.5, the medium carbon steel ranks first according to both yielding and leak-before-break criteria. For these

Table 9.3 Ranking of Several Metal Alloys Relative to Maximum Allowable Pressure (Leak-Before-Break Criterion) for a Thin-Walled Spherical Pressure Vessel

| <i>Material</i> | $\frac{K_{Ic}^2}{\sigma_y} (MPa\cdot m)$ |
|----------------------------------|--|
| Medium carbon (1040) steel | 11.2 |
| 4140 steel (tempered @ 482°C) | 6.1 |
| Ti-5Al-2.5Sn titanium | 5.8 |
| 2024 aluminum (T3) | 5.6 |
| 4340 steel (tempered @ 425°C) | 5.4 |
| 17-7PH steel | 4.4 |
| AZ31B magnesium | 3.9 |
| Ti-6Al-4V titanium | 3.3 |
| 4140 steel (tempered @ 370°C) | 2.4 |
| 4340 steel (tempered @ 260°C) | 1.5 |
| 7075 aluminum (T651) | 1.2 |

reasons, many pressure vessels are constructed of medium carbon steels, when temperature extremes and corrosion need not be considered.

9.6 BRITTLE FRACTURE OF CERAMICS

At room temperature, both crystalline and noncrystalline ceramics almost always fracture before any plastic deformation can occur in response to an applied tensile load. Furthermore, the mechanics of brittle fracture and principles of fracture mechanics developed earlier in this chapter also apply to the fracture of this group of materials.

It should be noted that stress raisers in brittle ceramics may be minute surface or interior cracks (microcracks), internal pores, and grain corners, which are virtually impossible to eliminate or control. For example, even moisture and contaminants in the atmosphere can introduce surface cracks in freshly drawn glass fibers; these cracks deleteriously affect the strength. In addition, plane strain fracture toughness values for ceramic materials are smaller than for metals; typically they are below $10 \text{ MPa}\sqrt{\text{m}}$ ($9 \text{ ksi}\sqrt{\text{in.}}$). Values of K_{Ic} for several ceramic materials are included in Table 9.1 and Table B.5, Appendix B.



There is usually considerable variation and scatter in the fracture strength for many specimens of a specific brittle ceramic material. A distribution of fracture strengths for portland cement is shown in Figure 9.16. This phenomenon may be explained by the dependence of fracture strength on the probability of the existence of a flaw that is capable of initiating a crack. This probability varies from specimen to specimen of the same material and depends on fabrication technique and any subsequent treatment. Specimen size or volume also influences fracture strength; the larger the specimen, the greater this flaw existence probability, and the lower the fracture strength.

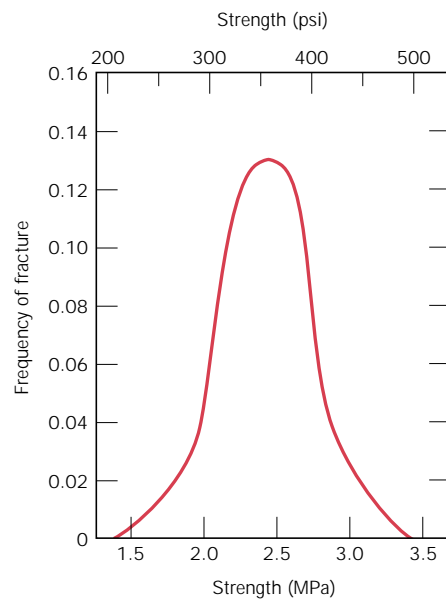


FIGURE 9.16 The frequency distribution of observed fracture strengths for a portland cement. (From W. Weibull, *Ing. Vetensk. Akad., Proc.* 151, No. 153, 1939.)

For compressive stresses, there is no stress amplification associated with any existent flaws. For this reason, brittle ceramics display much higher strengths in compression than in tension (on the order of a factor of 10), and they are generally utilized when load conditions are compressive. Also, the fracture strength of a brittle ceramic may be enhanced dramatically by imposing residual compressive stresses at its surface. {One way this may be accomplished is by thermal tempering (see Section 14.7).}

Statistical theories have been developed that in conjunction with experimental data are used to determine the risk of fracture for a given material; a discussion of these is beyond the scope of the present treatment. However, due to the dispersion in the measured fracture strengths of brittle ceramic materials, average values and factors of safety as discussed in Sections 7.19 and 7.20 are not normally employed for design purposes.

STATIC FATIGUE (CD-ROM)

9.7 FRACTURE OF POLYMERS

The fracture strengths of polymeric materials are low relative to those of metals and ceramics. As a general rule, the mode of fracture in thermosetting polymers is brittle. In simple terms, associated with the fracture process is the formation of cracks at regions where there is a localized stress concentration (i.e., scratches, notches, and sharp flaws). Covalent bonds in the network or crosslinked structure are severed during fracture.

For thermoplastic polymers, both ductile and brittle modes are possible, and many of these materials are capable of experiencing a ductile-to-brittle transition. Factors that favor brittle fracture are a reduction in temperature, an increase in strain rate, the presence of a sharp notch, increased specimen thickness, and, in addition, a modification of the polymer structure (chemical, molecular, and/or

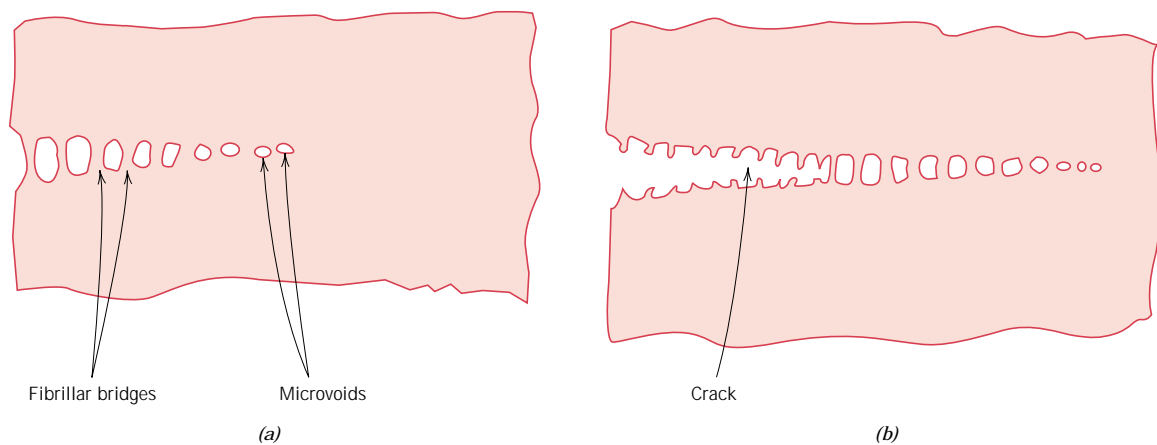


FIGURE 9.17 Schematic drawings of (a) a craze showing microvoids and fibrillar bridges, and (b) a craze followed by a crack. (From J. W. S. Hearle, *Polymers and Their Properties*, Vol. 1, *Fundamentals of Structure and Mechanics*, Ellis Horwood, Ltd., Chichester, West Sussex, England, 1982.)

microstructural). Glassy thermoplastics are brittle at relatively low temperatures; as the temperature is raised, they become ductile in the vicinity of their glass transition temperatures and experience plastic yielding prior to fracture. This behavior is demonstrated by the stress–strain characteristics of polymethyl methacrylate in Figure 7.24. At 4°C, PMMA is totally brittle, whereas at 60°C it becomes extremely ductile.

One phenomenon that frequently precedes fracture in some glassy thermoplastic polymers is *crazing*. Associated with crazes are regions of very localized yielding, which lead to the formation of small and interconnected microvoids (Figure 9.17a). Fibrillar bridges form between these microvoids wherein molecular chains become oriented. If the applied tensile load is sufficient, these bridges elongate and break, causing the microvoids to grow and coalesce; as the microvoids coalesce, cracks begin to form, as demonstrated in Figure 9.17b. A craze is different from a crack in that it can support a load across its face. Furthermore, this process of craze growth prior to cracking absorbs fracture energy and effectively increases the fracture toughness of the polymer. Crazes form at highly stressed regions associated with scratches, flaws, and molecular inhomogeneities; in addition, they propagate perpendicular to the applied tensile stress, and typically are 5 μm or less thick. Figure 9.18 is a photomicrograph in which a craze is shown.

Principles of fracture mechanics developed in Section 9.5 also apply to brittle and quasi-brittle polymers. The magnitude of K_{Ic} will depend on characteristics of the polymer (i.e., molecular weight, percent crystallinity, etc.) as well as temperature, strain rate, and the external environment. Representative values of K_{Ic} for several polymers are included in Table 9.1 and Table B.5, Appendix B.



9.8 IMPACT FRACTURE TESTING

Prior to the advent of fracture mechanics as a scientific discipline, impact testing techniques were established so as to ascertain the fracture characteristics of materials. It was realized that the results of laboratory tensile tests could not be extrapolated to predict fracture behavior; for example, under some circumstances normally

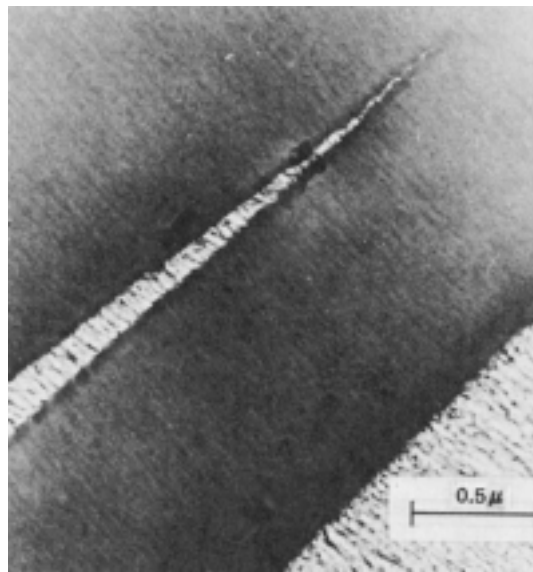


FIGURE 9.18 Photomicrograph of a craze in polyphenylene oxide. (From R. P. Kambour and R. E. Robertson, “The Mechanical Properties of Plastics,” in *Polymer Science, A Materials Science Handbook*, A. D. Jenkins, Editor. Reprinted with permission of Elsevier Science Publishers.)

ductile metals fracture abruptly and with very little plastic deformation. Impact test conditions were chosen to represent those most severe relative to the potential for fracture, namely, (1) deformation at a relatively low temperature, (2) a high strain rate (i.e., rate of deformation), and (3) a triaxial stress state (which may be introduced by the presence of a notch).

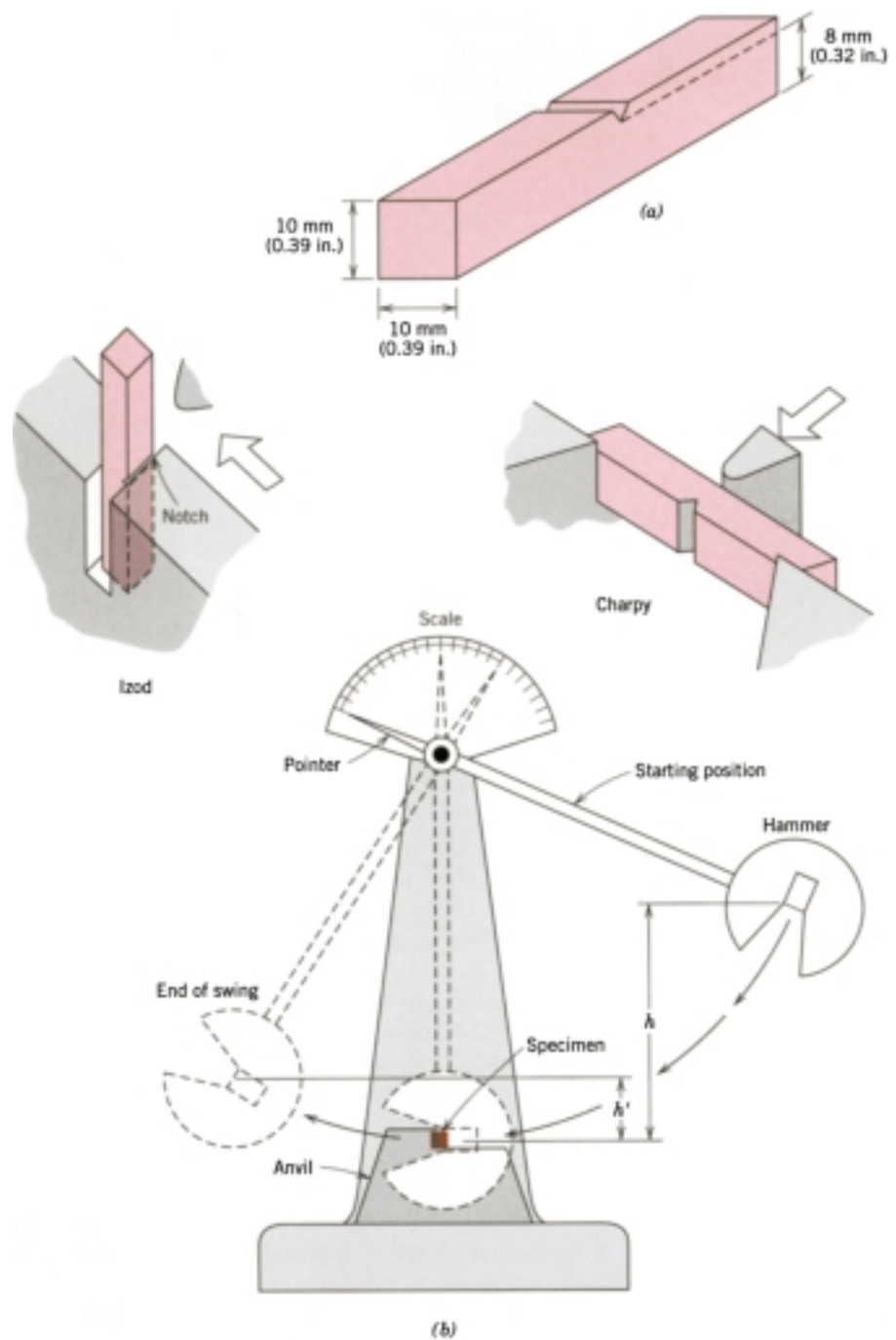
IMPACT TESTING TECHNIQUES

Two standardized tests,⁷ the **Charpy** and **Izod**, were designed and are still used to measure the **impact energy**, sometimes also termed *notch toughness*. The Charpy V-notch (CVN) technique is most commonly used in the United States. For both Charpy and Izod, the specimen is in the shape of a bar of square cross section, into which a V-notch is machined (Figure 9.19a). The apparatus for making V-notch impact tests is illustrated schematically in Figure 9.19b. The load is applied as an impact blow from a weighted pendulum hammer that is released from a cocked position at a fixed height h . The specimen is positioned at the base as shown. Upon release, a knife edge mounted on the pendulum strikes and fractures the specimen at the notch, which acts as a point of stress concentration for this high velocity impact blow. The pendulum continues its swing, rising to a maximum height h' , which is lower than h . The energy absorption, computed from the difference between h and h' , is a measure of the impact energy. The primary difference between the Charpy and Izod techniques lies in the manner of specimen support, as illustrated in Figure 9.19b. Furthermore, these are termed impact tests in light of the manner of load application. Variables including specimen size and shape as well as notch configuration and depth influence the test results.

Both plane strain fracture toughness and these impact tests determine the fracture properties of materials. The former are quantitative in nature, in that a specific property of the material is determined (i.e., K_{Ic}). The results of the impact

⁷ ASTM Standard E 23, “Standard Test Methods for Notched Bar Impact Testing of Metallic Materials.”

FIGURE 9.19 (a) Specimen used for Charpy and Izod impact tests. (b) A schematic drawing of an impact testing apparatus. The hammer is released from fixed height h and strikes the specimen; the energy expended in fracture is reflected in the difference between h and the swing height h' . Specimen placements for both Charpy and Izod tests are also shown. (Figure (b) adapted from H. W. Hayden, W. G. Moffatt, and J. Wulff, *The Structure and Properties of Materials*, Vol. III, *Mechanical Behavior*, p. 13. Copyright © 1965 by John Wiley & Sons, New York. Reprinted by permission of John Wiley & Sons, Inc.)



tests, on the other hand, are more qualitative and are of little use for design purposes. Impact energies are of interest mainly in a relative sense and for making comparisons—absolute values are of little significance. Attempts have been made to correlate plane strain fracture toughnesses and CVN energies, with only limited success. Plane strain fracture toughness tests are not as simple to perform as impact tests; furthermore, equipment and specimens are more expensive.

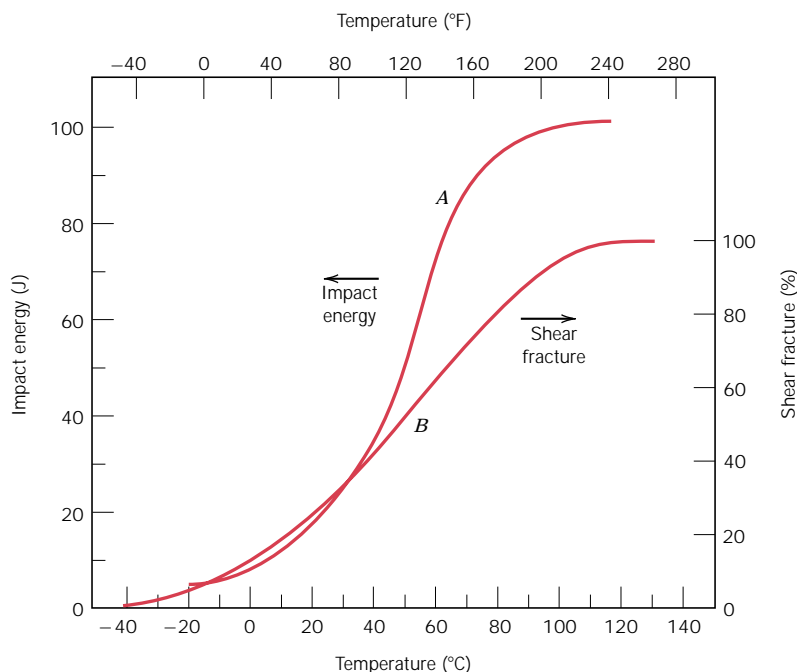
DUCTILE-TO-BRITTLE TRANSITION

One of the primary functions of Charpy and Izod tests is to determine whether or not a material experiences a **ductile-to-brittle transition** with decreasing temperature and, if so, the range of temperatures over which it occurs. The ductile-to-brittle transition is related to the temperature dependence of the measured impact energy absorption. This transition is represented for a steel by curve *A* in Figure 9.20. At higher temperatures the CVN energy is relatively large, in correlation with a ductile mode of fracture. As the temperature is lowered, the impact energy drops suddenly over a relatively narrow temperature range, below which the energy has a constant but small value; that is, the mode of fracture is brittle.

Alternatively, appearance of the failure surface is indicative of the nature of fracture, and may be used in transition temperature determinations. For ductile fracture this surface appears fibrous or dull (or of shear character); conversely, totally brittle surfaces have a granular (shiny) texture (or cleavage character). Over the ductile-to-brittle transition, features of both types will exist (Figure 9.21). Frequently, the percent shear fracture is plotted as a function of temperature—curve *B* in Figure 9.20.

For many alloys there is a range of temperatures over which the ductile-to-brittle transition occurs (Figure 9.20); this presents some difficulty in specifying a single ductile-to-brittle transition temperature. No explicit criterion has been established, and so this temperature is often defined as that temperature at which the CVN energy assumes some value (e.g., 20 J or 15 ft-lb_f), or corresponding to some given fracture appearance (e.g., 50% fibrous fracture). Matters are further complicated inasmuch as a different transition temperature may be realized for each of these criteria. Perhaps the most conservative transition temperature is that at which the fracture surface becomes 100% fibrous; on this basis, the transition temperature is approximately 110°C (230°F) for the steel alloy that is the subject of Figure 9.20.

FIGURE 9.20
Temperature dependence of the Charpy V-notch impact energy (curve *A*) and percent shear fracture (curve *B*) for an A283 steel. (Reprinted from *Welding Journal*. Used by permission of the American Welding Society.)



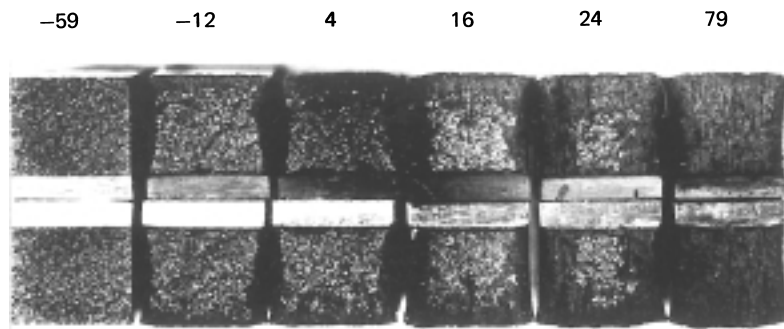


FIGURE 9.21 Photograph of fracture surfaces of A36 steel Charpy V-notch specimens tested at indicated temperatures (in °C). (From R. W. Hertzberg, *Deformation and Fracture Mechanics of Engineering Materials*, 3rd edition, Fig. 9.6, p. 329. Copyright © 1989 by John Wiley & Sons, Inc., New York. Reprinted by permission of John Wiley & Sons, Inc.)

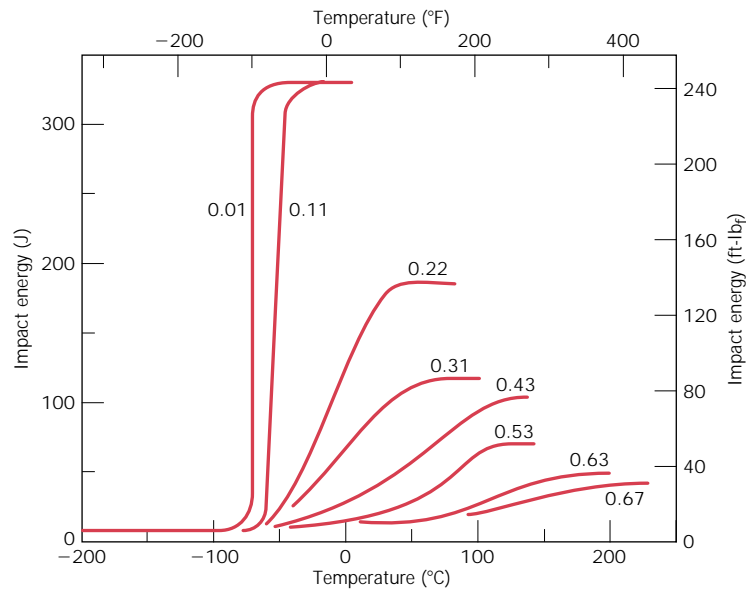
Structures constructed from alloys that exhibit this ductile-to-brittle behavior should be used only at temperatures above the transition temperature, to avoid brittle and catastrophic failure. Classic examples of this type of failure occurred, with disastrous consequences, during World War II when a number of welded transport ships, away from combat, suddenly and precipitously split in half. The vessels were constructed of a steel alloy that possessed adequate ductility according to room-temperature tensile tests. The brittle fractures occurred at relatively low ambient temperatures, at about 4°C (40°F), in the vicinity of the transition temperature of the alloy. Each fracture crack originated at some point of stress concentration, probably a sharp corner or fabrication defect, and then propagated around the entire girth of the ship.

Not all metal alloys display a ductile-to-brittle transition. Those having FCC crystal structures (including aluminum- and copper-based alloys) remain ductile even at extremely low temperatures. However, BCC and HCP alloys experience this transition. For these materials the transition temperature is sensitive to both alloy composition and microstructure. For example, decreasing the average grain size of steels results in a lowering of the transition temperature. Hence, refining the grain size both strengthens (Section 8.9) and toughens steels. In contrast, increasing the carbon content, while increasing the strength of steels, also raises the CVN transition of steels, as indicated in Figure 9.22.

Izod or Charpy tests are also conducted to assess impact strength of polymeric materials. As with metals, polymers may exhibit ductile or brittle fracture under impact loading conditions, depending on the temperature, specimen size, strain rate, and mode of loading, as discussed in the preceding section. Both semicrystalline and amorphous polymers are brittle at low temperatures, and both have relatively low impact strengths. However, they experience a ductile-to-brittle transition over a relatively narrow temperature range, similar to that shown for a steel in Figure 9.20. Of course, impact strength undergoes a gradual decrease at still higher temperatures as the polymer begins to soften. Ordinarily, the two impact characteristics most sought after are a high impact strength at the ambient temperature and a ductile-to-brittle transition temperature that lies below room temperature.

Most ceramics also experience a ductile-to-brittle transition, which occurs only at elevated temperatures—ordinarily in excess of 1000°C (1850°F).

FIGURE 9.22 Influence of carbon content on the Charpy V-notch energy-versus-temperature behavior for steel. (Reprinted with permission from ASM International, Metals Park, OH 44073-9989, USA; J. A. Reinbolt and W. J. Harris, Jr., “Effect of Alloying Elements on Notch Toughness of Pearlitic Steels,” *Transactions of ASM*, Vol. 43, 1951.)



FATIGUE

Fatigue is a form of failure that occurs in structures subjected to dynamic and fluctuating stresses (e.g., bridges, aircraft, and machine components). Under these circumstances it is possible for failure to occur at a stress level considerably lower than the tensile or yield strength for a static load. The term “fatigue” is used because this type of failure normally occurs after a lengthy period of repeated stress or strain cycling. Fatigue is important inasmuch as it is the single largest cause of failure in metals, estimated to comprise approximately 90% of all metallic failures; polymers and ceramics (except for glasses) are also susceptible to this type of failure. Furthermore, it is catastrophic and insidious, occurring very suddenly and without warning.

Fatigue failure is brittlelike in nature even in normally ductile metals, in that there is very little, if any, gross plastic deformation associated with failure. The process occurs by the initiation and propagation of cracks, and ordinarily the fracture surface is perpendicular to the direction of an applied tensile stress.

9.9 CYCLIC STRESSES

The applied stress may be axial (tension-compression), flexural (bending), or torsional (twisting) in nature. In general, three different fluctuating stress–time modes are possible. One is represented schematically by a regular and sinusoidal time dependence in Figure 9.23a, wherein the amplitude is symmetrical about a mean zero stress level, for example, alternating from a maximum tensile stress (σ_{\max}) to a minimum compressive stress (σ_{\min}) of equal magnitude; this is referred to as a *reversed stress cycle*. Another type, termed *repeated stress cycle*, is illustrated in Figure 9.23b; the maxima and minima are asymmetrical relative to the zero stress level. Finally, the stress level may vary randomly in amplitude and frequency, as exemplified in Figure 9.23c.

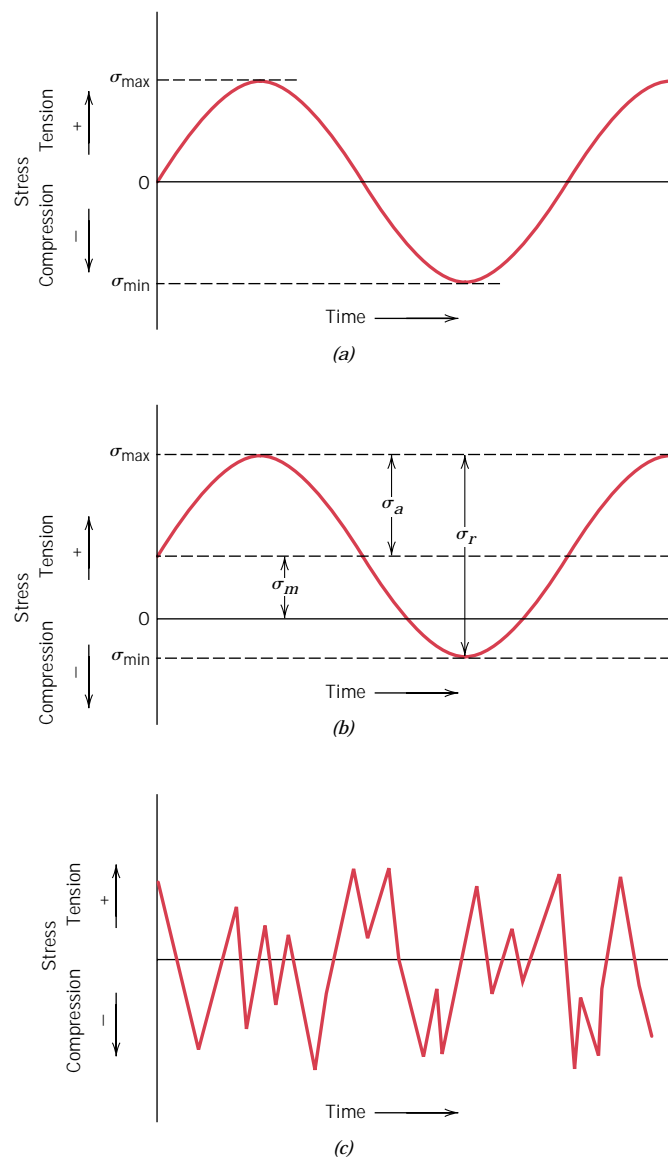


FIGURE 9.23 Variation of stress with time that accounts for fatigue failures. (a) Reversed stress cycle, in which the stress alternates from a maximum tensile stress (+) to a maximum compressive stress (−) of equal magnitude. (b) Repeated stress cycle, in which maximum and minimum stresses are asymmetrical relative to the zero stress level; mean stress σ_m , range of stress σ_r , and stress amplitude σ_a are indicated. (c) Random stress cycle.

Also indicated in Figure 9.23b are several parameters used to characterize the fluctuating stress cycle. The stress amplitude alternates about a *mean stress* σ_m , defined as the average of the maximum and minimum stresses in the cycle, or

$$\sigma_m = \frac{\sigma_{\max} + \sigma_{\min}}{2} \quad (9.21)$$

Furthermore, the *range of stress* σ_r is just the difference between σ_{\max} and σ_{\min} , namely,

$$\sigma_r = \sigma_{\max} - \sigma_{\min} \quad (9.22)$$

Stress amplitude σ_a is just one half of this range of stress, or

$$\sigma_a = \frac{\sigma_r}{2} = \frac{\sigma_{\max} - \sigma_{\min}}{2} \quad (9.23)$$

Finally, the *stress ratio* R is just the ratio of minimum and maximum stress amplitudes:

$$R = \frac{\sigma_{\min}}{\sigma_{\max}} \quad (9.24)$$

By convention, tensile stresses are positive and compressive stresses are negative. For example, for the reversed stress cycle, the value of R is -1 .

9.10 THE S-N CURVE

As with other mechanical characteristics, the fatigue properties of materials can be determined from laboratory simulation tests.⁸ A test apparatus should be designed to duplicate as nearly as possible the service stress conditions (stress level, time frequency, stress pattern, etc.). A schematic diagram of a rotating-bending test apparatus, commonly used for fatigue testing, is shown in Figure 9.24; the compression and tensile stresses are imposed on the specimen as it is simultaneously bent and rotated. Tests are also frequently conducted using an alternating uniaxial tension-compression stress cycle.

A series of tests are commenced by subjecting a specimen to the stress cycling at a relatively large maximum stress amplitude (σ_{\max}), usually on the order of two thirds of the static tensile strength; the number of cycles to failure is counted. This procedure is repeated on other specimens at progressively decreasing maximum stress amplitudes. Data are plotted as stress S versus the logarithm of the number N of cycles to failure for each of the specimens. The values of S are normally taken as stress amplitudes (σ_a , Equation 9.23); on occasion, σ_{\max} or σ_{\min} values may be used.

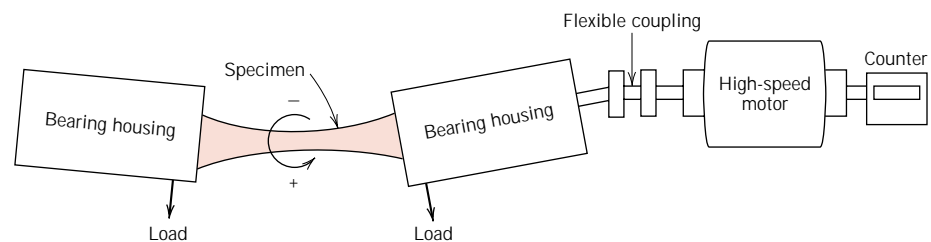
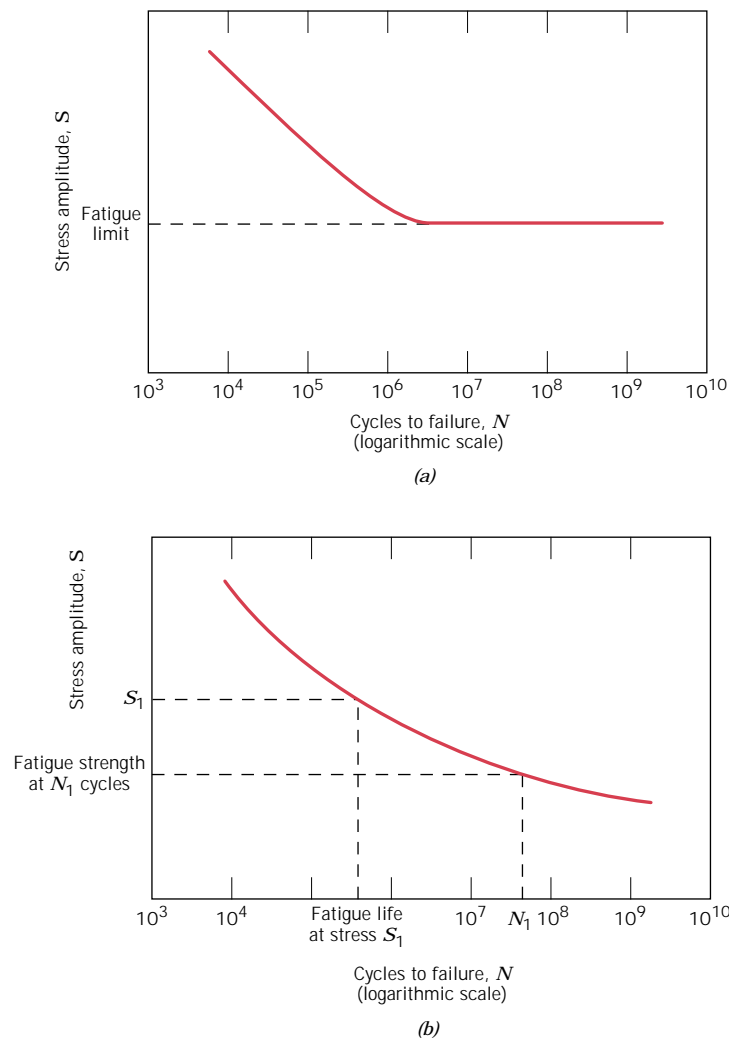


FIGURE 9.24 Schematic diagram of fatigue testing apparatus for making rotating-bending tests. (From *Materials Science in Engineering*, fourth edition, by Keyser, Carl A., © 1986. Reprinted by permission of Prentice-Hall, Inc., Upper Saddle River, NJ.)

⁸ See ASTM Standard E 466, "Standard Practice for Conducting Constant Amplitude Axial Fatigue Tests of Metallic Materials," and ASTM Standard E 468, "Standard Practice for Presentation of Constant Amplitude Fatigue Test Results for Metallic Materials."

FIGURE 9.25 Stress amplitude (S) versus logarithm of the number of cycles to fatigue failure (N) for (a) a material that displays a fatigue limit, and (b) a material that does not display a fatigue limit.



Two distinct types of S - N behavior are observed, which are represented schematically in Figure 9.25. As these plots indicate, the higher the magnitude of the stress, the smaller the number of cycles the material is capable of sustaining before failure. For some ferrous (iron base) and titanium alloys, the S - N curve (Figure 9.25a) becomes horizontal at higher N values; or, there is a limiting stress level, called the **fatigue limit** (also sometimes the *endurance limit*), below which fatigue failure will not occur. This fatigue limit represents the largest value of fluctuating stress that will *not* cause failure for essentially an infinite number of cycles. For many steels, fatigue limits range between 35 and 60% of the tensile strength.

Most nonferrous alloys (e.g., aluminum, copper, magnesium) do not have a fatigue limit, in that the S - N curve continues its downward trend at increasingly greater N values (Figure 9.25b). Thus, fatigue will ultimately occur regardless of the magnitude of the stress. For these materials, the fatigue response is specified as **fatigue strength**, which is defined as the stress level at which failure will occur

for some specified number of cycles (e.g., 10^7 cycles). The determination of fatigue strength is also demonstrated in Figure 9.25*b*.

Another important parameter that characterizes a material's fatigue behavior is **fatigue life** N_f . It is the number of cycles to cause failure at a specified stress level, as taken from the S - N plot (Figure 9.25*b*).

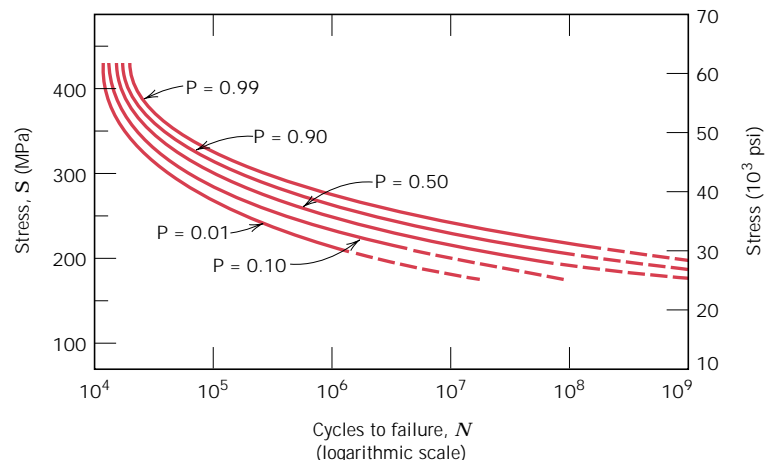
Unfortunately, there always exists considerable scatter in fatigue data, that is, a variation in the measured N value for a number of specimens tested at the same stress level. This may lead to significant design uncertainties when fatigue life and/or fatigue limit (or strength) are being considered. The scatter in results is a consequence of the fatigue sensitivity to a number of test and material parameters that are impossible to control precisely. These parameters include specimen fabrication and surface preparation, metallurgical variables, specimen alignment in the apparatus, mean stress, and test frequency.

Fatigue S - N curves similar to those shown in Figure 9.25 represent “best fit” curves which have been drawn through average-value data points. It is a little unsettling to realize that approximately one half of the specimens tested actually failed at stress levels lying nearly 25% below the curve (as determined on the basis of statistical treatments).

Several statistical techniques have been developed to specify fatigue life and fatigue limit in terms of probabilities. One convenient way of representing data treated in this manner is with a series of constant probability curves, several of which are plotted in Figure 9.26. The P value associated with each curve represents the probability of failure. For example, at a stress of 200 MPa (30,000 psi), we would expect 1% of the specimens to fail at about 10^6 cycles and 50% to fail at about 2×10^7 cycles, and so on. It should be remembered that S - N curves represented in the literature are normally average values, unless noted otherwise.

The fatigue behaviors represented in Figures 9.25*a* and 9.25*b* may be classified into two domains. One is associated with relatively high loads that produce not only elastic strain but also some plastic strain during each cycle. Consequently, fatigue lives are relatively short; this domain is termed *low-cycle fatigue* and occurs at less than about 10^4 to 10^5 cycles. For lower stress levels wherein deformations are totally elastic, longer lives result. This is called *high-cycle fatigue* inasmuch as relatively large numbers of cycles are required to produce

FIGURE 9.26 Fatigue S - N probability of failure curves for a 7075-T6 aluminum alloy; P denotes the probability of failure. (From G. M. Sinclair and T. J. Dolan, *Trans., ASME*, **75**, 1953, p. 867. Reprinted with permission of the American Society of Mechanical Engineers.)



fatigue failure. High-cycle fatigue is associated with fatigue lives greater than about 10^4 to 10^5 cycles.

9.11 FATIGUE IN POLYMERIC MATERIALS

Polymers may experience fatigue failure under conditions of cyclic loading. As with metals, fatigue occurs at stress levels that are low relative to the yield strength. Fatigue data are plotted in the same manner for both types of material, and the resulting curves have the same general shape. Fatigue curves for several common polymers are shown in Figure 9.27, as stress versus the number of cycles to failure (on a logarithmic scale). Some polymers have a fatigue limit. As would be expected, fatigue strengths and fatigue limits for polymeric materials are much lower than for metals.

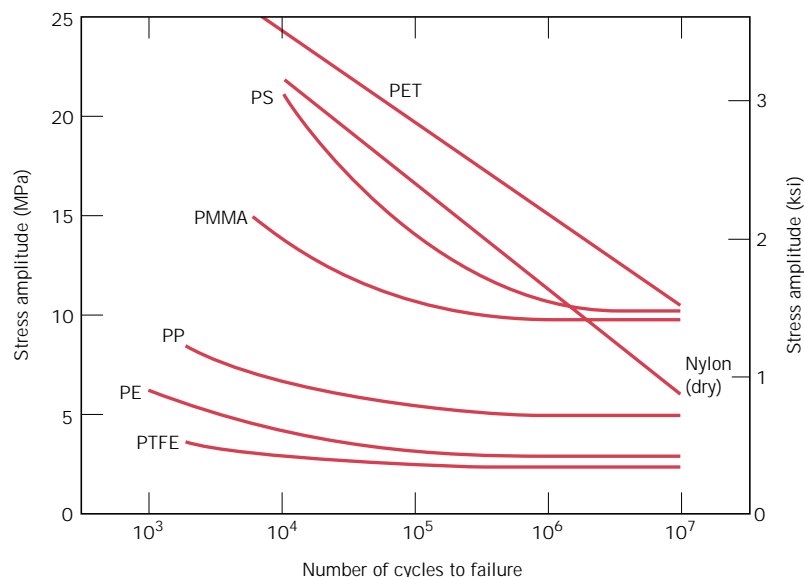
The fatigue behavior of polymers is much more sensitive to loading frequency than for metals. Cycling polymers at high frequencies and/or relatively large stresses can cause localized heating; consequently, failure may be due to a softening of the material rather than as a result of typical fatigue processes.

9.12a CRACK INITIATION AND PROPAGATION [DETAILED VERSION (CD-ROM)]

9.12b CRACK INITIATION AND PROPAGATION (CONCISE VERSION)

The process of fatigue failure is characterized by three distinct steps: (1) crack initiation, wherein a small crack forms at some point of high stress concentration; (2) crack propagation, during which this crack advances incrementally with each stress cycle; and (3) final failure, which occurs very rapidly once the advancing

FIGURE 9.27 Fatigue curves (stress amplitude versus the number of cycles to failure) for polyethylene terephthalate (PET), nylon, polystyrene (PS), polymethyl methacrylate (PMMA), polypropylene (PP), polyethylene (PE), and polytetrafluoroethylene (PTFE). The testing frequency was 30 Hz. (From M. N. Riddell, "A Guide to Better Testing of Plastics," *Plast. Eng.*, Vol. 30, No. 4, p. 78, 1974.)



crack has reached a critical size. Cracks associated with fatigue failure almost always initiate (or nucleate) on the surface of a component at some point of stress concentration. Crack nucleation sites include surface scratches, sharp fillets, keyways, threads, dents, and the like. In addition, cyclic loading can produce microscopic surface discontinuities resulting from dislocation slip steps which may also act as stress raisers, and therefore as crack initiation sites.

The region of a fracture surface that formed during the crack propagation step may be characterized by two types of markings termed *beachmarks* and *striations*. Both of these features indicate the position of the crack tip at some point in time and appear as concentric ridges that expand away from the crack initiation site(s), frequently in a circular or semicircular pattern. Beachmarks (sometimes also called “clamshell marks”) are of macroscopic dimensions (Figure 9.30), and may be observed with the unaided eye. These markings are found for components that experienced interruptions during the crack propagation stage—for example, a machine that operated only during normal work-shift hours. Each beachmark band represents a period of time over which crack growth occurred.

On the other hand, fatigue striations are microscopic in size and subject to observation with the electron microscope (either TEM or SEM). Figure 9.31 is an electron fractograph which shows this feature. Each striation is thought to represent the advance distance of a crack front during a single load cycle. Striation width depends on, and increases with, increasing stress range.

At this point it should be emphasized that although both beachmarks and striations are fatigue fracture surface features having similar appearances, they are nevertheless different, both in origin and size. There may be literally thousands of striations within a single beachmark.

Often the cause of failure may be deduced after examination of the failure surfaces. The presence of beachmarks and/or striations on a fracture surface con-

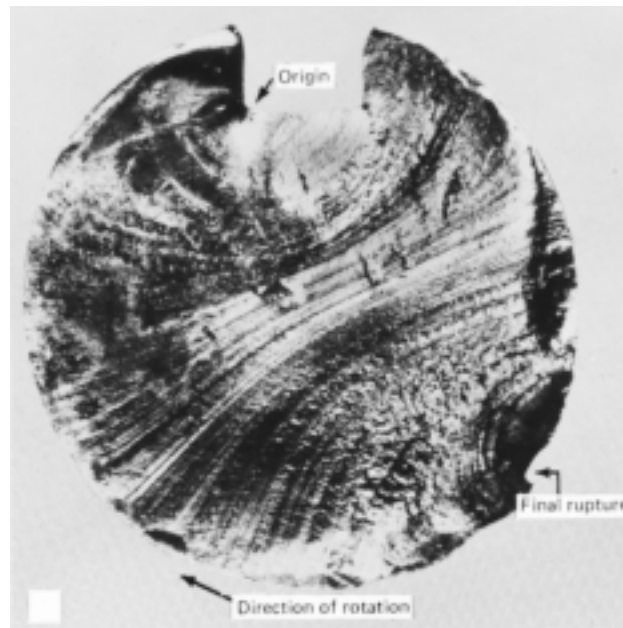


FIGURE 9.30 Fracture surface of a rotating steel shaft that experienced fatigue failure. Beachmark ridges are visible in the photograph. (Reproduced with permission from D. J. Wulpi, *Understanding How Components Fail*, American Society for Metals, Materials Park, OH, 1985.)



FIGURE 9.31 Transmission electron fractograph showing fatigue striations in aluminum. Magnification unknown. (From V. J. Colangelo and F. A. Heiser, *Analysis of Metallurgical Failures*, 2nd edition. Copyright © 1987 by John Wiley & Sons, New York. Reprinted by permission of John Wiley & Sons, Inc.)

firms that the cause of failure was fatigue. Nevertheless, the absence of either or both does not exclude fatigue as the cause of failure.

One final comment regarding fatigue failure surfaces: Beachmarks and striations will not appear on that region over which the rapid failure occurs. Rather, the rapid failure may be either ductile or brittle; evidence of plastic deformation will be present for ductile, and absent for brittle, failure. This region of failure may be noted in Figure 9.32.

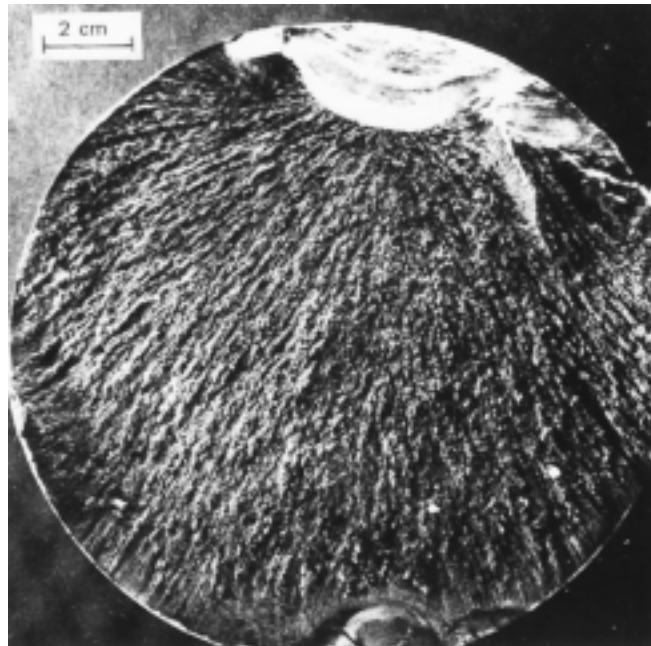


FIGURE 9.32 Fatigue failure surface. A crack formed at the top edge. The smooth region also near the top corresponds to the area over which the crack propagated slowly. Rapid failure occurred over the area having a dull and fibrous texture (the largest area). Approximately $0.5\times$. (Reproduced by permission from *Metals Handbook: Fractography and Atlas of Fractographs*, Vol. 9, 8th edition, H. E. Boyer, Editor, American Society for Metals, 1974.)

9.13 CRACK PROPAGATION RATE (CD-ROM)

9.14 FACTORS THAT AFFECT FATIGUE LIFE

As was mentioned in Section 9.10, the fatigue behavior of engineering materials is highly sensitive to a number of variables. Some of these factors include mean stress level, geometrical design, surface effects, and metallurgical variables, as well as the environment. This section is devoted to a discussion of these factors and, in addition, to measures that may be taken to improve the fatigue resistance of structural components.

MEAN STRESS

The dependence of fatigue life on stress amplitude is represented on the S - N plot. Such data are taken for a constant mean stress σ_m , often for the reversed cycle situation ($\sigma_m = 0$). Mean stress, however, will also affect fatigue life, which influence may be represented by a series of S - N curves, each measured at a different σ_m ; this is depicted schematically in Figure 9.36. As may be noted, increasing the mean stress level leads to a decrease in fatigue life.

SURFACE EFFECTS

For many common loading situations, the maximum stress within a component or structure occurs at its surface. Consequently, most cracks leading to fatigue failure originate at surface positions, specifically at stress amplification sites. Therefore, it has been observed that fatigue life is especially sensitive to the condition and configuration of the component surface. Numerous factors influence fatigue resistance, the proper management of which will lead to an improvement in fatigue life. These include design criteria as well as various surface treatments.

Design Factors

The design of a component can have a significant influence on its fatigue characteristics. Any notch or geometrical discontinuity can act as a stress raiser and fatigue crack initiation site; these design features include grooves, holes, keyways, threads, and so on. The sharper the discontinuity (i.e., the smaller the radius of curvature),

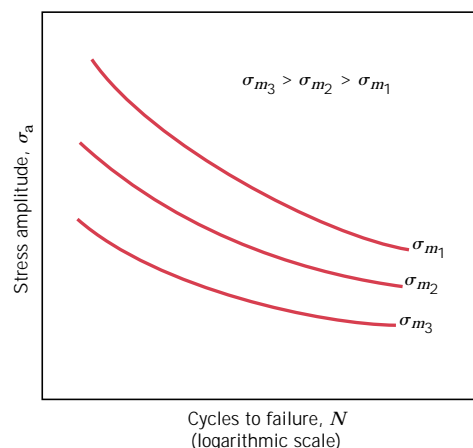


FIGURE 9.36 Demonstration of influence of mean stress σ_m on S - N fatigue behavior.

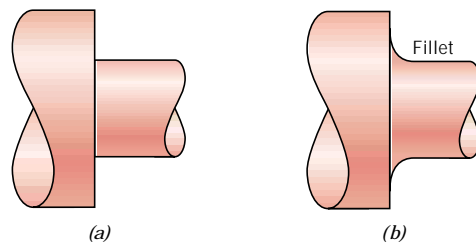


FIGURE 9.37 Demonstration of how design can reduce stress amplification. (a) Poor design: sharp corner. (b) Good design: fatigue lifetime improved by incorporating rounded fillet into a rotating shaft at the point where there is a change in diameter.

the more severe the stress concentration. The probability of fatigue failure may be reduced by avoiding (when possible) these structural irregularities, or by making design modifications whereby sudden contour changes leading to sharp corners are eliminated—for example, calling for rounded fillets with large radii of curvature at the point where there is a change in diameter for a rotating shaft (Figure 9.37).

Surface Treatments

During machining operations, small scratches and grooves are invariably introduced into the workpiece surface by cutting tool action. These surface markings can limit the fatigue life. It has been observed that improving the surface finish by polishing will enhance fatigue life significantly.

One of the most effective methods of increasing fatigue performance is by imposing residual compressive stresses within a thin outer surface layer. Thus, a surface tensile stress of external origin will be partially nullified and reduced in magnitude by the residual compressive stress. The net effect is that the likelihood of crack formation and therefore of fatigue failure is reduced.

Residual compressive stresses are commonly introduced into ductile metals mechanically by localized plastic deformation within the outer surface region. Commercially, this is often accomplished by a process termed *shot peening*. Small, hard particles (shot) having diameters within the range of 0.1 to 1.0 mm are projected at high velocities onto the surface to be treated. The resulting deformation induces compressive stresses to a depth of between one quarter and one half of the shot diameter. The influence of shot peening on the fatigue behavior of steel is demonstrated schematically in Figure 9.38.

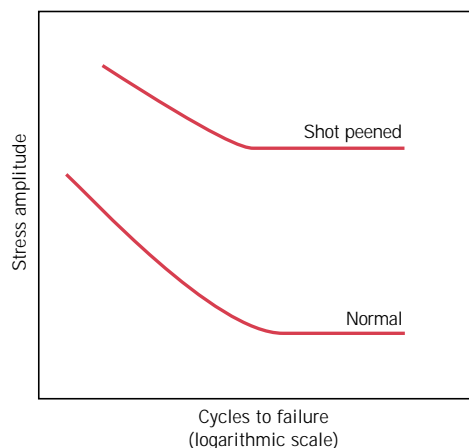


FIGURE 9.38 Schematic S - N fatigue curves for normal and shot-peened steel.

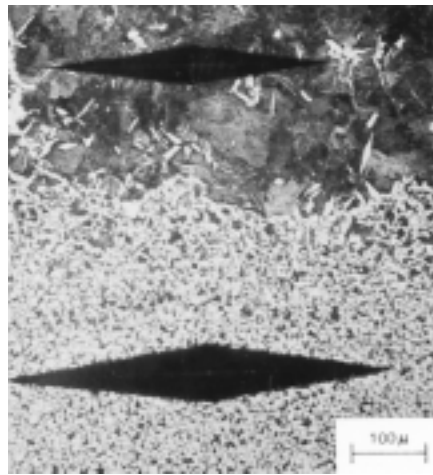


FIGURE 9.39 Photomicrograph showing both core (bottom) and carburized outer case (top) regions of a case-hardened steel. The case is harder as attested by the smaller microhardness indentation. 100 \times . (From R. W. Hertzberg, *Deformation and Fracture Mechanics of Engineering Materials*, 3rd edition. Copyright © 1989 by John Wiley & Sons, New York. Reprinted by permission of John Wiley & Sons, Inc.)

Case hardening is a technique whereby both surface hardness and fatigue life are enhanced for steel alloys. This is accomplished by a carburizing or nitriding process whereby a component is exposed to a carbonaceous or nitrogenous atmosphere at an elevated temperature. A carbon- or nitrogen-rich outer surface layer (or “case”) is introduced by atomic diffusion from the gaseous phase. The case is normally on the order of 1 mm deep and is harder than the inner core of material. (The influence of carbon content on hardness for Fe–C alloys is demonstrated in Figure 11.21a.) The improvement of fatigue properties results from increased hardness within the case, as well as the desired residual compressive stresses the formation of which attends the carburizing or nitriding process. A carbon-rich outer case may be observed for the gear shown in the chapter-opening photograph for Chapter 6; it appears as a dark outer rim within the sectioned segment. The increase in case hardness is demonstrated in the photomicrograph appearing in Figure 9.39. The dark and elongated diamond shapes are Knoop microhardness indentations. The upper indentation, lying within the carburized layer, is smaller than the core indentation.

9.15 ENVIRONMENTAL EFFECTS (CD-ROM)

CREEP

Materials are often placed in service at elevated temperatures and exposed to static mechanical stresses (e.g., turbine rotors in jet engines and steam generators that experience centrifugal stresses, and high-pressure steam lines). Deformation under such circumstances is termed **creep**. Defined as the time-dependent and permanent deformation of materials when subjected to a constant load or stress, creep is normally an undesirable phenomenon and is often the limiting factor in the lifetime of a part. It is observed in all materials types; for metals it becomes important only for temperatures greater than about $0.4 T_m$ (T_m = absolute melting temperature).

9.16 GENERALIZED CREEP BEHAVIOR

A typical creep test¹⁰ consists of subjecting a specimen to a constant load or stress while maintaining the temperature constant; deformation or strain is measured and plotted as a function of elapsed time. Most tests are the constant load type, which yield information of an engineering nature; constant stress tests are employed to provide a better understanding of the mechanisms of creep.

Figure 9.40 is a schematic representation of the typical constant load creep behavior of metals. Upon application of the load there is an instantaneous deformation, as indicated in the figure, which is mostly elastic. The resulting creep curve consists of three regions, each of which has its own distinctive strain–time feature. *Primary* or *transient creep* occurs first, typified by a continuously decreasing creep rate; that is, the slope of the curve diminishes with time. This suggests that the material is experiencing an increase in creep resistance or strain hardening (Section 8.11)—deformation becomes more difficult as the material is strained. For *secondary creep*, sometimes termed *steady-state creep*, the rate is constant; that is, the plot becomes linear. This is often the stage of creep that is of the longest duration. The constancy of creep rate is explained on the basis of a balance between the competing processes of strain hardening and recovery, recovery (Section 8.12) being the process whereby a material becomes softer and retains its ability to experience deformation. Finally, for *tertiary creep*, there is an acceleration of the rate and ultimate failure. This failure is frequently termed *rupture* and results from microstructural and/or metallurgical changes; for example, grain boundary separation, and the formation of internal cracks, cavities, and voids. Also, for tensile loads, a neck may form at some point within the deformation region. These all lead to a decrease in the effective cross-sectional area and an increase in strain rate.

For metallic materials most creep tests are conducted in uniaxial tension using a specimen having the same geometry as for tensile tests (Figure 7.2). On the other hand, uniaxial compression tests are more appropriate for brittle materials; these provide a better measure of the intrinsic creep properties inasmuch as there is no stress amplification and crack propagation, as with tensile loads. Compressive test specimens are usually right cylinders or parallelepipeds having length-to-diameter

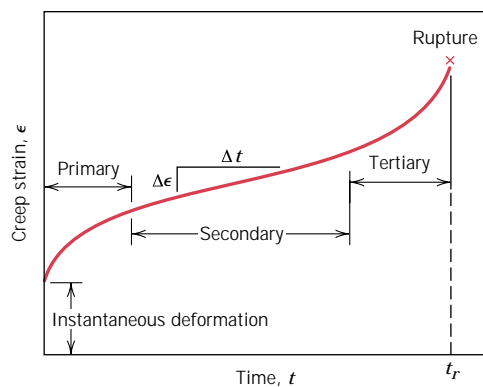


FIGURE 9.40 Typical creep curve of strain versus time at constant stress and constant elevated temperature. The minimum creep rate $\Delta\epsilon/\Delta t$ is the slope of the linear segment in the secondary region. Rupture lifetime t_r is the total time to rupture.

¹⁰ ASTM Standard E 139, “Standard Practice for Conducting Creep, Creep-Rupture, and Stress-Rupture Tests of Metallic Materials.”

ratios ranging from about 2 to 4. For most materials creep properties are virtually independent of loading direction.

Possibly the most important parameter from a creep test is the slope of the secondary portion of the creep curve ($\Delta\epsilon/\Delta t$ in Figure 9.40); this is often called the minimum or *steady-state creep rate* $\dot{\epsilon}_s$. It is the engineering design parameter that is considered for long-life applications, such as a nuclear power plant component that is scheduled to operate for several decades, and when failure or too much strain is not an option. On the other hand, for many relatively short-life creep situations (e.g., turbine blades in military aircraft and rocket motor nozzles), *time to rupture*, or the *rupture lifetime* t_r , is the dominant design consideration; it is also indicated in Figure 9.40. Of course, for its determination, creep tests must be conducted to the point of failure; these are termed *creep rupture* tests. Thus, a knowledge of these creep characteristics of a material allows the design engineer to ascertain its suitability for a specific application.

9.17a STRESS AND TEMPERATURE EFFECTS [DETAILED VERSION (CD-ROM)]

9.17b STRESS AND TEMPERATURE EFFECTS (CONCISE VERSION)

Both temperature and the level of the applied stress influence the creep characteristics (Figure 9.41). At a temperature substantially below $0.4 T_m$, and after the initial deformation, the strain is virtually independent of time. With either increasing stress or temperature, the following will be noted: (1) the instantaneous strain at the time of stress application increases; (2) the steady-state creep rate is increased; and (3) the rupture lifetime is diminished.

The results of creep rupture tests are most commonly presented as the logarithm of stress versus the logarithm of rupture lifetime. Figure 9.42 is one such plot for a nickel alloy in which a linear relationship can be seen to exist at each temperature. For some alloys and over relatively large stress ranges, nonlinearity in these curves is observed.

Both temperature and stress effects on the steady-state creep rate are represented graphically as logarithm of stress versus logarithm of $\dot{\epsilon}_s$ for tests conducted

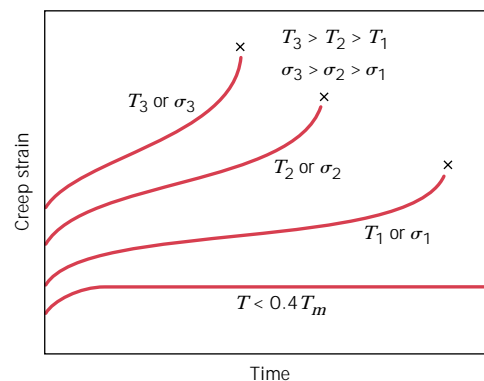


FIGURE 9.41 Influence of stress σ and temperature T on creep behavior.

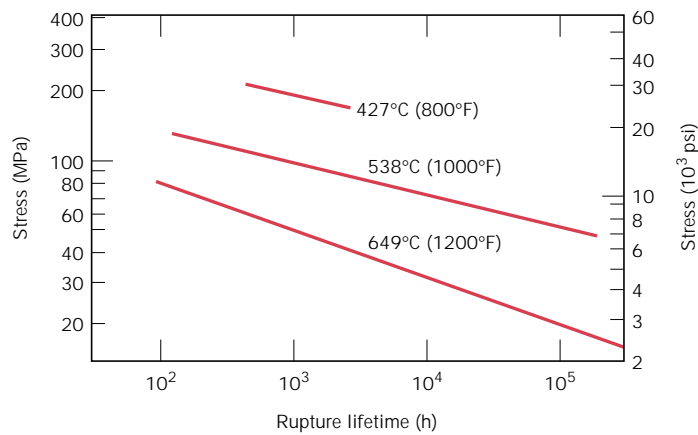


FIGURE 9.42 Stress (logarithmic scale) versus rupture lifetime (logarithmic scale) for a low carbon–nickel alloy at three temperatures. (From *Metals Handbook: Properties and Selection: Stainless Steels, Tool Materials and Special-Purpose Metals*, Vol. 3, 9th edition, D. Benjamin, Senior Editor, American Society for Metals, 1980, p. 130.)

at a variety of temperatures. Figure 9.43 shows data that were collected at three temperatures for the same nickel alloy. Clearly, a straight line segment is drawn at each temperature.

9.18 DATA EXTRAPOLATION METHODS (CD-ROM)

9.19 ALLOYS FOR HIGH-TEMPERATURE USE

There are several factors that affect the creep characteristics of metals. These include melting temperature, elastic modulus, and grain size. In general, the higher the melting temperature, the greater the elastic modulus, and the larger the grain

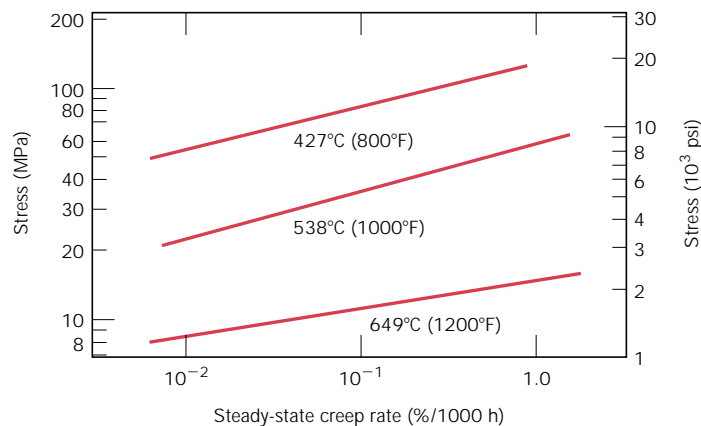


FIGURE 9.43 Stress (logarithmic scale) versus steady-state creep rate (logarithmic scale) for a low carbon–nickel alloy at three temperatures. (From *Metals Handbook: Properties and Selection: Stainless Steels, Tool Materials and Special-Purpose Metals*, Vol. 3, 9th edition, D. Benjamin, Senior Editor, American Society for Metals, 1980, p. 131.)

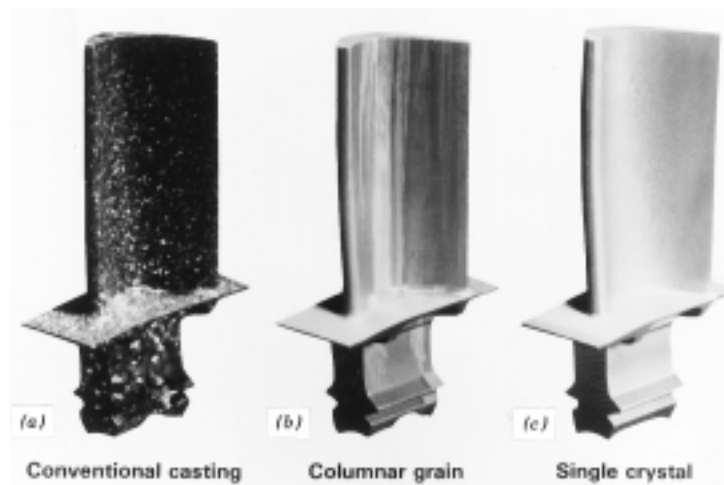


FIGURE 9.45 (a) Polycrystalline turbine blade that was produced by a conventional casting technique. High-temperature creep resistance is improved as a result of an oriented columnar grain structure (b) produced by a sophisticated directional solidification technique. Creep resistance is further enhanced when single-crystal blades (c) are used. (Courtesy of Pratt & Whitney.)

size, the better is a material's resistance to creep. Relative to grain size, smaller grains permit more grain-boundary sliding, which results in higher creep rates. This effect may be contrasted to the influence of grain size on the mechanical behavior at low temperatures [i.e., increase in both strength (Section 8.9) and toughness (Section 9.8)].

Stainless steels (Section 13.2), the refractory metals and the superalloys (Section 13.3) are especially resilient to creep and are commonly employed in high-temperature service applications. The creep resistance of the cobalt and nickel superalloys is enhanced by solid-solution alloying, and also by the addition of a dispersed phase which is virtually insoluble in the matrix. In addition, advanced processing techniques have been utilized; one such technique is directional solidification, which produces either highly elongated grains or single-crystal components (Figure 9.45). Another is the controlled unidirectional solidification of alloys having specially designed compositions wherein two-phase composites result.

9.20 CREEP IN CERAMIC AND POLYMERIC MATERIALS

Ceramic materials often experience creep deformation as a result of exposure to stresses (usually compressive) at elevated temperatures. In general, the time-deformation creep behavior of ceramics is similar to that of metals (Figure 9.40); however, creep occurs at higher temperatures in ceramics.

Viscoelastic creep is the term used to denote the creep phenomenon in polymeric materials. {It is one of the topics of discussion in Section 7.15.}

SUMMARY

Fracture, in response to tensile loading and at relatively low temperatures, may occur by ductile and brittle modes, both of which involve the formation and propagation of

cracks. For ductile fracture, evidence will exist of gross plastic deformation at the fracture surface. In tension, highly ductile metals will neck down to essentially a point fracture; cup-and-cone mating fracture surfaces result for moderate ductility. {Microscopically, dimples (spherical and parabolic) are produced.} Cracks in ductile materials are said to be stable (i.e., resist extension without an increase in applied stress); and inasmuch as fracture is noncatastrophic, this fracture mode is almost always preferred.

For brittle fracture, cracks are unstable, and the fracture surface is relatively flat and perpendicular to the direction of the applied tensile load. Chevron and ridgelike patterns are possible, which indicate the direction of crack propagation. Transgranular (through-grain) and intergranular (between-grain) fractures are found in brittle polycrystalline materials.

The discipline of fracture mechanics allows for a better understanding of the fracture process and provides for structural design wherein the probability of failure is minimized. The significant discrepancy between actual and theoretical fracture strengths of brittle materials is explained by the existence of small flaws that are capable of amplifying an applied tensile stress in their vicinity, leading ultimately to crack formation. Stress amplification is greatest for long flaws that have small tip radii of curvature. Fracture ensues when the theoretical cohesive strength is exceeded at the tip of one of these flaws. Consideration of elastic strain and crack surface energies gives rise to an expression for a crack propagation critical stress in brittle materials; this parameter is a function of elastic modulus, specific surface energy, and crack length.

{The stress distributions in front of an advancing crack may be expressed in terms of position (as radial and angular coordinates) as well as stress intensity factor.} The critical value of the stress intensity factor (i.e., that at which fracture occurs) is termed the fracture toughness, which is related to stress level, crack length, and a geometrical factor. The fracture toughness of a material is indicative of its resistance to brittle fracture when a crack is present. It depends on specimen thickness, and, for relatively thick specimens (i.e., conditions of plane strain), is termed the plane strain fracture toughness. This parameter is the one normally cited for design purposes; its value is relatively large for ductile materials (and small for brittle ones), and is a function of microstructure, strain rate, and temperature. With regard to designing against the possibility of fracture, consideration must be given to material (its fracture toughness), the stress level, and the flaw size detection limit.

At room temperature, virtually all ceramics are brittle. Microcracks, the presence of which is very difficult to control, result in amplification of applied tensile stresses and account for relatively low fracture strengths (flexural strengths). This amplification does not occur with compressive loads, and, consequently, ceramics are stronger in compression.

Fracture strengths of polymeric materials are also low relative to metals. Both brittle and ductile fracture modes are possible, and some thermoplastic materials experience a ductile-to-brittle transition with a lowering of temperature, an increase in strain rate, and/or an alteration of specimen thickness or geometry. In some glassy thermoplastics, the crack formation process may be preceded by crazing; crazing can lead to an increase in ductility and toughness of the material.

Qualitatively, the fracture behavior of materials may be determined using Charpy and Izod impact testing techniques; impact energy (or notch toughness) is measured for specimens into which a V-shaped notch has been machined. On the basis of the temperature dependence of this impact energy (or appearance of the

fracture surface), it is possible to ascertain whether or not a material experiences a ductile-to-brittle transition and the temperature range over which such a transition occurs. Metal alloys having BCC and HCP crystal structures experience this transition, and, for structural applications, should be used at temperatures in excess of this transition range.

Fatigue is a common type of catastrophic failure wherein the applied stress level fluctuates with time. Test data are plotted as stress versus the logarithm of the number of cycles to failure. For many materials, the number of cycles to failure increases continuously with diminishing stress. Fatigue strength represents the failure stress for a specified number of cycles. For some steels and titanium alloys, stress ceases to decrease with, and becomes independent of, the number of cycles; fatigue limit is the magnitude of this constant stress level, below which fatigue will not occur even for virtually an infinite number of cycles. Another fatigue property is fatigue life, which, for a specific stress, is the number of cycles to failure.

As a result of significant scatter in measured fatigue data, statistical analyses are performed that lead to specification of fatigue life and limit in terms of probabilities.

The processes of fatigue crack initiation and propagation were discussed. Cracks normally nucleate on the surface of a component at some point of stress concentration. Propagation proceeds in two stages, which are characterized by propagation direction and rate. {The mechanism for the more rapid stage II corresponds to a repetitive plastic blunting and sharpening process at the advancing crack tip.}

Two characteristic fatigue surface features are beachmarks and striations. Beachmarks form on components that experience applied stress interruptions; they normally may be observed with the naked eye. Fatigue striations are of microscopic dimensions, and each is thought to represent the crack tip advance distance over a single load cycle.

{An analytical expression was proposed for fatigue crack propagation rate in terms of the stress intensity range at the crack tip. Integration of the expression yields an equation whereby fatigue life may be estimated.}

Measures that may be taken to extend fatigue life include (1) reducing the mean stress level, (2) eliminating sharp surface discontinuities, (3) improving the surface finish by polishing, (4) imposing surface residual compressive stresses by shot peening, and (5) case hardening by using a carburizing or nitriding process.

{The fatigue behavior of materials may also be affected by the environment. Thermal stresses may be induced in components that are exposed to elevated temperature fluctuations and when thermal expansion and/or contraction is restrained; fatigue for these conditions is termed thermal fatigue. The presence of a chemically active environment may lead to a reduction in fatigue life for corrosion fatigue; small pit crack nucleation sites form on the component surface as a result of chemical reactions.}

The time-dependent plastic deformation of materials subjected to a constant load (or stress) and temperatures greater than about $0.4T_m$ is termed creep. A typical creep curve (strain versus time) will normally exhibit three distinct regions. For transient (or primary) creep, the rate (or slope) diminishes with time. The plot becomes linear (i.e., creep rate is constant) in the steady-state (or secondary) region. And finally, deformation accelerates for tertiary creep, just prior to failure (or rupture). Important design parameters available from such a plot include the steady-state creep rate (slope of the linear region) and rupture lifetime.

Both temperature and applied stress level influence creep behavior. Increasing either of these parameters produces the following effects: (1) an increase in the instantaneous initial deformation, (2) an increase in the steady-state creep rate,

and (3) a diminishment of the rupture lifetime. {Analytical expressions were presented which relate $\dot{\epsilon}_s$ to both temperature and stress. Creep mechanisms may be discerned on the basis of steady-state rate stress exponent and creep activation energy values.}

{Extrapolation of creep test data to lower temperature–longer time regimes is possible using the Larson–Miller parameter.}

Metal alloys that are especially resistant to creep have high elastic moduli and melting temperatures; these include the superalloys, the stainless steels, and the refractory metals. Various processing techniques are employed to improve the creep properties of these materials.

The creep phenomenon is also observed in ceramic and polymeric materials.

IMPORTANT TERMS AND CONCEPTS

| | | |
|-------------------------------|------------------------|---------------------------------|
| Brittle fracture | Fatigue life | Izod test |
| Case hardening | Fatigue limit | Plane strain |
| Charpy test | Fatigue strength | Plane strain fracture toughness |
| Corrosion fatigue | Fracture mechanics | Stress intensity factor |
| Creep | Fracture toughness | Stress raiser |
| Ductile fracture | Impact energy | Thermal fatigue |
| Ductile-to-brittle transition | Intergranular fracture | Transgranular fracture |
| Fatigue | | |

REFERENCES

- ASM Handbook*, Vol. 11, *Failure Analysis and Prevention*, ASM International, Materials Park, OH, 1986.
- ASM Handbook*, Vol. 12, *Fractography*, ASM International, Materials Park, OH, 1987.
- Boyer, H. E. (Editor), *Atlas of Creep and Stress–Rupture Curves*, ASM International, Materials Park, OH, 1988.
- Boyer, H. E. (Editor), *Atlas of Fatigue Curves*, ASM International, Materials Park, OH, 1986.
- Colangelo, V. J. and F. A. Heiser, *Analysis of Metallurgical Failures*, 2nd edition, John Wiley & Sons, New York, 1987.
- Collins, J. A., *Failure of Materials in Mechanical Design*, 2nd edition, John Wiley & Sons, New York, 1993.
- Courtney, T. H., *Mechanical Behavior of Materials*, McGraw-Hill Book Co., New York, 1990.
- Davidge, R. W., *Mechanical Behaviour of Ceramics*, Cambridge University Press, Cambridge, 1979. Reprinted by TechBooks, Marietta, OH.
- Dieter, G. E., *Mechanical Metallurgy*, 3rd edition, McGraw-Hill Book Co., New York, 1986.
- Esaklul, K. A., *Handbook of Case Histories in Failure Analysis*, ASM International, Materials Park, OH, 1992 and 1993. In two volumes.
- Fatigue Data Book: Light Structural Alloys*, ASM International, Materials Park, OH, 1995.
- Hertzberg, R. W., *Deformation and Fracture Mechanics of Engineering Materials*, 4th edition, John Wiley & Sons, New York, 1996.
- Murakami, Y. (Editor), *Stress Intensity Factors Handbook*, Pergamon Press, Oxford, 1987. In two volumes.
- Tetelman, A. S. and A. J. McEvily, *Fracture of Structural Materials*, John Wiley & Sons, New York, 1967. Reprinted by Books on Demand, Ann Arbor, MI.
- Wachtman, J. B., *Mechanical Properties of Ceramics*, John Wiley & Sons, Inc., New York, 1996.
- Ward, I. M. and D. W. Hadley, *An Introduction to the Mechanical Properties of Solid Polymers*, John Wiley & Sons, Chichester, UK, 1993.

Wulpi, D. J., *Understanding How Components Fail*, American Society for Metals, Materials Park, OH, 1985.

Young, R. J. and P. Lovell, *Introduction to Polymers*, 2nd edition, Chapman and Hall, London, 1991.

QUESTIONS AND PROBLEMS

Note: To solve those problems having an asterisk (*) by their numbers, consultation of supplementary topics [appearing only on the CD-ROM (and not in print)] will probably be necessary.

- 9.1** Cite at least two situations in which the possibility of failure is part of the design of a component or product.
- 9.2*** Estimate the theoretical cohesive strengths of the ceramic materials listed in Table 7.1.
- 9.3** What is the magnitude of the maximum stress that exists at the tip of an internal crack having a radius of curvature of 2.5×10^{-4} mm (10^{-5} in.) and a crack length of 2.5×10^{-2} mm (10^{-3} in.) when a tensile stress of 170 MPa (25,000 psi) is applied?
- 9.4** Estimate the theoretical fracture strength of a brittle material if it is known that fracture occurs by the propagation of an elliptically shaped surface crack of length 0.25 mm (0.01 in.) and having a tip radius of curvature of 1.2×10^{-3} mm (4.7×10^{-5} in.) when a stress of 1200 MPa (174,000 psi) is applied.
- 9.5*** A specimen of a ceramic material having a modulus of elasticity of 300 GPa (43.5×10^6 psi) is pulled in tension with a stress of 900 MPa (130,000 psi). Will the specimen fail if its “most severe flaw” is an internal crack that has a length of 0.30 mm (0.012 in.) and a tip radius of curvature of 5×10^{-4} mm (2×10^{-5} in.)? Why or why not?
- 9.6** Briefly explain (a) why there may be significant scatter in the fracture strength for some given ceramic material, and (b) why fracture strength increases with decreasing specimen size.
- 9.7** The tensile strength of brittle materials may be determined using a variation of Equation 9.1b. Compute the critical crack tip radius for an Al_2O_3 specimen that experiences tensile fracture at an applied stress of 275 MPa (40,000 psi). Assume a critical surface crack length of 2×10^{-3} mm and a theoretical

fracture strength of $E/10$, where E is the modulus of elasticity.

- 9.8** If the specific surface energy for soda-lime glass is 0.30 J/m^2 , using data contained in Table 7.1, compute the critical stress required for the propagation of a surface crack of length 0.05 mm.
- 9.9** A polystyrene component must not fail when a tensile stress of 1.25 MPa (180 psi) is applied. Determine the maximum allowable surface crack length if the surface energy of polystyrene is 0.50 J/m^2 (2.86×10^{-3} in.-lb_f/in.²). Assume a modulus of elasticity of 3.0 GPa (0.435×10^6 psi).
- 9.10*** The parameter K in Equations 9.7a, 9.7b, and 9.7c is a function of the applied nominal stress σ and crack length a as

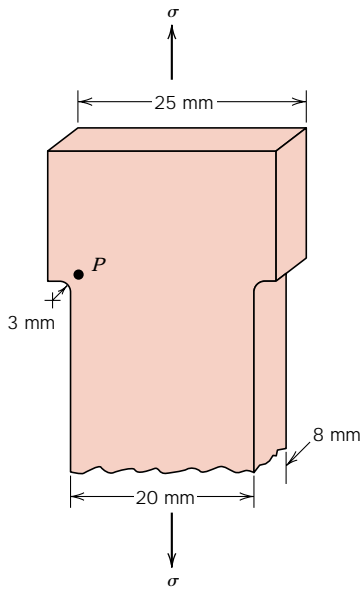
$$K = \sigma \sqrt{\pi a}$$

Compute the magnitudes of the normal stresses σ_x and σ_y in front of a surface crack of length 2.5 mm (0.10 in.) (as depicted in Figure 9.10) in response to a nominal tensile stress of 75 MPa (10,875 psi) at the following positions:

- (a) $r = 0.15 \text{ mm}$ (6.0×10^{-3} in.), $\theta = 30^\circ$
 (b) $r = 0.15 \text{ mm}$ (6.0×10^{-3} in.), $\theta = 60^\circ$
 (c) $r = 0.75 \text{ mm}$ (3.0×10^{-2} in.), $\theta = 30^\circ$
 (d) $r = 0.75 \text{ mm}$ (3.0×10^{-2} in.), $\theta = 60^\circ$
- 9.11*** The parameter K in Equations 9.7a, 9.7b, and 9.7c is defined in the previous problem.
- (a) For a surface crack of length 3.0 mm (0.118 in.), determine the radial position at an angle θ of 45° at which the normal stress σ_x is 110 MPa (16,000 psi) when the magnitude of the nominal applied stress is 100 MPa (14,500 psi).

(b) Compute the normal stress σ_y at this same position.

9.12* A portion of a tensile specimen is shown as follows:



(a) Compute the magnitude of the stress at point P when the externally applied stress is 100 MPa (14,500 psi).

(b) How much will the radius of curvature at point P have to be increased to reduce this stress by 20%?

9.13* A cylindrical hole 25 mm (1.0 in.) in diameter passes entirely through the thickness of a steel plate 15 mm (0.6 in.) thick, 100 mm (4 in.) wide, and 400 mm (15.75 in.) long (see Figure 9.8a).

(a) Calculate the stress at the edge of this hole when a tensile stress of 50 MPa (7250 psi) is applied in a lengthwise direction.

(b) Calculate the stress at the hole edge when the same stress in part (a) is applied in a widthwise direction.

9.14* Cite the significant differences between the stress intensity factor, the plane stress fracture toughness, and the plane strain fracture toughness.

9.15* For each of the metal alloys listed in Table 9.1, compute the minimum component thickness for which the condition of plane strain is valid.

9.16 A specimen of a 4340 steel alloy having a plane strain fracture toughness of $45 \text{ MPa}\sqrt{\text{m}}$ ($41 \text{ ksi}\sqrt{\text{in.}}$) is exposed to a stress of 1000 MPa (145,000 psi). Will this specimen experience fracture if it is known that the largest surface crack is 0.75 mm (0.03 in.) long? Why or why not? Assume that the parameter Y has a value of 1.0.

9.17 Some aircraft component is fabricated from an aluminum alloy that has a plane strain fracture toughness of $35 \text{ MPa}\sqrt{\text{m}}$ ($31.9 \text{ ksi}\sqrt{\text{in.}}$). It has been determined that fracture results at a stress of 250 MPa (36,250 psi) when the maximum (or critical) internal crack length is 2.0 mm (0.08 in.). For this same component and alloy, will fracture occur at a stress level of 325 MPa (47,125 psi) when the maximum internal crack length is 1.0 mm (0.04 in.)? Why or why not?

9.18 Suppose that a wing component on an aircraft is fabricated from an aluminum alloy that has a plane strain fracture toughness of $40 \text{ MPa}\sqrt{\text{m}}$ ($36.4 \text{ ksi}\sqrt{\text{in.}}$). It has been determined that fracture results at a stress of 365 MPa (53,000 psi) when the maximum internal crack length is 2.5 mm (0.10 in.). For this same component and alloy, compute the stress level at which fracture will occur for a critical internal crack length of 4.0 mm (0.16 in.).

9.19 A large plate is fabricated from a steel alloy that has a plane strain fracture toughness of $55 \text{ MPa}\sqrt{\text{m}}$ ($50 \text{ ksi}\sqrt{\text{in.}}$). If, during service use, the plate is exposed to a tensile stress of 200 MPa (29,000 psi), determine the minimum length of a surface crack that will lead to fracture. Assume a value of 1.0 for Y .

9.20 Calculate the maximum internal crack length allowable for a 7075-T651 aluminum alloy (Table 9.1) component that is loaded to a stress one half of its yield strength. Assume that the value of Y is 1.35.

9.21 A structural component in the form of a wide plate is to be fabricated from a steel alloy that has a plane strain fracture toughness of $77 \text{ MPa}\sqrt{\text{m}}$ ($70.1 \text{ ksi}\sqrt{\text{in.}}$) and a yield strength of 1400 MPa (205,000 psi). The flaw size resolution limit of the flaw detection apparatus is 4.0 mm (0.16 in.). If the design stress is one half of the yield strength and

the value of Y is 1.0, determine whether or not a critical flaw for this plate is subject to detection.

- 9.22*** A structural component in the shape of a flat plate 12.5 mm (0.5 in.) thick is to be fabricated from a metal alloy for which the yield strength and plane strain fracture toughness values are 350 MPa (50,750 psi) and $33 \text{ MPa}\sqrt{\text{m}}$ ($30 \text{ ksi}\sqrt{\text{in.}}$), respectively; for this particular geometry, the value of Y is 1.75. Assuming a design stress of one half of the yield strength, is it possible to compute the critical length of a surface flaw? If so, determine its length; if this computation is not possible from the given data, then explain why.
- 9.23** After consultation of other references, write a brief report on one or two nondestructive test techniques that are used to detect and measure internal and/or surface flaws in metal alloys.
- 9.24** The fracture strength of glass may be increased by etching away a thin surface layer. It is believed that the etching may alter surface crack geometry (i.e., reduce crack length and increase the tip radius). Compute the ratio of the original and etched crack tip radii for an eightfold increase in fracture strength if two-thirds of the crack length is removed.
- 9.25** For thermoplastic polymers, cite five factors that favor brittle fracture.
- 9.26** Tabulated below are data that were gathered from a series of Charpy impact tests on a ductile cast iron:

| Temperature (°C) | Impact Energy (J) |
|------------------|-------------------|
| -25 | 124 |
| -50 | 123 |
| -75 | 115 |
| -85 | 100 |
| -100 | 73 |
| -110 | 52 |
| -125 | 26 |
| -150 | 9 |
| -175 | 6 |

- (a) Plot the data as impact energy versus temperature.
- (b) Determine a ductile-to-brittle transition temperature as that temperature corre-

sponding to the average of the maximum and minimum impact energies.

(c) Determine a ductile-to-brittle transition temperature as that temperature at which the impact energy is 80 J.

- 9.27** Tabulated as follows are data that were gathered from a series of Charpy impact tests on a tempered 4140 steel alloy:

| Temperature (°C) | Impact Energy (J) |
|------------------|-------------------|
| 100 | 89.3 |
| 75 | 88.6 |
| 50 | 87.6 |
| 25 | 85.4 |
| 0 | 82.9 |
| -25 | 78.9 |
| -50 | 73.1 |
| -65 | 66.0 |
| -75 | 59.3 |
| -85 | 47.9 |
| -100 | 34.3 |
| -125 | 29.3 |
| -150 | 27.1 |
| -175 | 25.0 |

- (a) Plot the data as impact energy versus temperature.
- (b) Determine a ductile-to-brittle transition temperature as that temperature corresponding to the average of the maximum and minimum impact energies.
- (c) Determine a ductile-to-brittle transition temperature as that temperature at which the impact energy is 70 J.
- 9.28** Briefly explain why BCC and HCP metal alloys may experience a ductile-to-brittle transition with decreasing temperature, whereas FCC alloys do not experience such a transition.
- 9.29** A fatigue test was conducted in which the mean stress was 50 MPa (7250 psi) and the stress amplitude was 225 MPa (32,625 psi).
- (a) Compute the maximum and minimum stress levels.
- (b) Compute the stress ratio.
- (c) Compute the magnitude of the stress range.
- 9.30** A cylindrical 1045 steel bar (Figure 9.46) is subjected to repeated compression-tension stress cycling along its axis. If the load ampli-

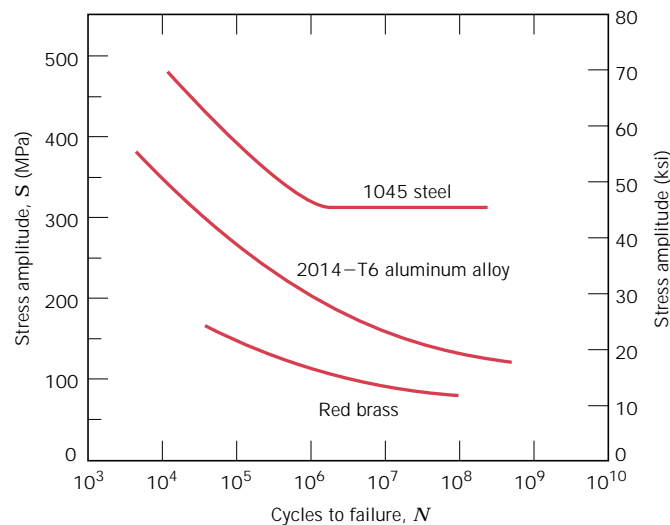


FIGURE 9.46 Stress magnitude S versus the logarithm of the number N of cycles to fatigue failure for red brass, an aluminum alloy, and a plain carbon steel. (Adapted from H. W. Hayden, W. G. Moffatt, and J. Wulff, *The Structure and Properties of Materials*, Vol. III, *Mechanical Behavior*, p. 15. Copyright © 1965 by John Wiley & Sons, New York. Reprinted by permission of John Wiley & Sons, Inc. Also adapted from *ASM Handbook*, Vol. 2, *Properties and Selection: Nonferrous Alloys and Special-Purpose Materials*, 1990. Reprinted by permission of ASM International.)

tude is 22,000 N (4950 lb_f), compute the minimum allowable bar diameter to ensure that fatigue failure will not occur. Assume a factor of safety of 2.0.

- 9.31** An 8.0 mm (0.31 in.) diameter cylindrical rod fabricated from a red brass alloy (Figure 9.46) is subjected to reversed tension-compression load cycling along its axis. If the maximum tensile and compressive loads are +7500 N (1700 lb_f) and -7500 N (-1700 lb_f), respectively, determine its fatigue life. Assume that the stress plotted in Figure 9.46 is stress amplitude.
- 9.32** A 12.5 mm (0.50 in.) diameter cylindrical rod fabricated from a 2014-T6 alloy (Figure 9.46) is subjected to a repeated tension-compression load cycling along its axis. Compute the maximum and minimum loads that will be applied to yield a fatigue life of 1.0×10^7 cycles. Assume that the stress plotted on the vertical axis is stress amplitude, and data were taken for a mean stress of 50 MPa (7250 psi).

- 9.33** The fatigue data for a brass alloy are given as follows:

| Stress Amplitude (MPa) | Cycles to Failure |
|------------------------|-------------------|
| 310 | 2×10^5 |
| 223 | 1×10^6 |
| 191 | 3×10^6 |
| 168 | 1×10^7 |
| 153 | 3×10^7 |
| 143 | 1×10^8 |
| 134 | 3×10^8 |
| 127 | 1×10^9 |

(a) Make an S - N plot (stress amplitude versus logarithm cycles to failure) using these data.

(b) Determine the fatigue strength at 5×10^5 cycles.

(c) Determine the fatigue life for 200 MPa.

- 9.34** Suppose that the fatigue data for the brass alloy in Problem 9.33 were taken from torsional tests, and that a shaft of this alloy is to be used for a coupling that is attached to

an electric motor operating at 1500 rpm. Give the maximum torsional stress amplitude possible for each of the following lifetimes of the coupling: **(a)** 1 year, **(b)** 1 month, **(c)** 1 day, and **(d)** 2 hours.

9.35 The fatigue data for a ductile cast iron are given as follows:

| Stress Amplitude [MPa (ksi)] | Cycles to Failure |
|---------------------------------|----------------------|
| 248 (36.0) | 1×10^5 |
| 236 (34.2) | 3×10^5 |
| 224 (32.5) | 1×10^6 |
| 213 (30.9) | 3×10^6 |
| 201 (29.1) | 1×10^7 |
| 193 (28.0) | 3×10^7 |
| 193 (28.0) | 1×10^8 |
| 193 (28.0) | 3×10^8 |

(a) Make an $S-N$ plot (stress amplitude versus logarithm cycles to failure) using the data.

(b) What is the fatigue limit for this alloy?

(c) Determine fatigue lifetimes at stress amplitudes of 230 MPa (33,500 psi) and 175 MPa (25,000 psi).

(d) Estimate fatigue strengths at 2×10^5 and 6×10^6 cycles.

9.36 Suppose that the fatigue data for the cast iron in Problem 9.35 were taken for bending-rotating tests, and that a rod of this alloy is to be used for an automobile axle that rotates at an average rotational velocity of 750 revolutions per minute. Give maximum lifetimes of continuous driving that are allowable for the following stress levels: **(a)** 250 MPa (36,250 psi), **(b)** 215 MPa (31,000 psi), **(c)** 200 MPa (29,000 psi), and **(d)** 150 MPa (21,750 psi).

9.37 Three identical fatigue specimens (denoted A, B, and C) are fabricated from a nonferrous alloy. Each is subjected to one of the maximum-minimum stress cycles listed below; the frequency is the same for all three tests.

| Specimen | σ_{\max} (MPa) | σ_{\min} (MPa) |
|----------|-----------------------|-----------------------|
| A | +450 | -350 |
| B | +400 | -300 |
| C | +340 | -340 |

(a) Rank the fatigue lifetimes of these three specimens from the longest to the shortest.

(b) Now justify this ranking using a schematic $S-N$ plot.

9.38 (a) Compare the fatigue limits for polystyrene (Figure 9.27) and the cast iron for which fatigue data are given in Problem 9.35.

(b) Compare the fatigue strengths at 10^6 cycles for polyethylene terephthalate (PET, Figure 9.27) and red brass (Figure 9.46).

9.39 Cite five factors that may lead to scatter in fatigue life data.

9.40 Make a schematic sketch of the fatigue behavior for some metal for which the stress ratio R has a value of +1.

9.41 Using Equations 9.23 and 9.24, demonstrate that increasing the value of the stress ratio R produces a decrease in stress amplitude σ_a .

9.42 Surfaces for some steel specimens that have failed by fatigue have a bright crystalline or grainy appearance. Laymen may explain the failure by saying that the metal crystallized while in service. Offer a criticism for this explanation.

9.43 Briefly explain the difference between fatigue striations and beachmarks both in terms of **(a)** size and **(b)** origin.

9.44 List four measures that may be taken to increase the resistance to fatigue of a metal alloy.

9.45 Give the approximate temperature at which creep deformation becomes an important consideration for each of the following metals: nickel, copper, iron, tungsten, lead, and aluminum.

9.46 Superimpose on the same strain-versus-time plot schematic creep curves for both constant tensile stress and constant load, and explain the differences in behavior.

9.47 The following creep data were taken on an aluminum alloy at 400°C (750°F) and a constant stress of 25 MPa (3660 psi). Plot the data as strain versus time, then determine the steady-state or minimum creep rate. *Note:* The initial and instantaneous strain is not included.

| Time (min) | Strain | Time (min) | Strain |
|---------------|--------|---------------|--------|
| 0 | 0.000 | 16 | 0.135 |
| 2 | 0.025 | 18 | 0.153 |
| 4 | 0.043 | 20 | 0.172 |
| 6 | 0.065 | 22 | 0.193 |
| 8 | 0.078 | 24 | 0.218 |
| 10 | 0.092 | 26 | 0.255 |
| 12 | 0.109 | 28 | 0.307 |
| 14 | 0.120 | 30 | 0.368 |

- 9.48** A specimen 750 mm (30 in.) long of a low carbon–nickel alloy (Figure 9.43) is to be exposed to a tensile stress of 40 MPa (5800 psi) at 538°C (1000°F). Determine its elongation after 5000 h. Assume that the total of both instantaneous and primary creep elongations is 1.5 mm (0.06 in.).
- 9.49** For a cylindrical low carbon–nickel alloy specimen (Figure 9.43) originally 10 mm (0.40 in.) in diameter and 500 mm (20 in.) long, what tensile load is necessary to produce a total elongation of 3.2 mm (0.13 in.) after 10,000 h at 427°C (800°F)? Assume that the sum of instantaneous and primary creep elongations is 0.8 mm (0.03 in.).
- 9.50** If a component fabricated from a low carbon–nickel alloy (Figure 9.42) is to be exposed to a tensile stress of 60 MPa (8700 psi) at 538°C (1000°F), estimate its rupture lifetime.
- 9.51** A cylindrical component constructed from a low carbon–nickel alloy (Figure 9.42) has a diameter of 12 mm (0.50 in.). Determine the maximum load that may be applied for it to survive 500 h at 649°C (1200°F).
- 9.52*** From Equation 9.33, if the logarithm of $\dot{\epsilon}_s$ is plotted versus the logarithm of σ , then a straight line should result, the slope of which is the stress exponent n . Using Figure 9.43, determine the value of n for the low carbon–nickel alloy at each of the three temperatures.
- 9.53*** (a) Estimate the activation energy for creep (i.e., Q_c in Equation 9.34) for the low carbon–nickel alloy having the steady-state creep behavior shown in Figure 9.43. Use data taken at a stress level of 55 MPa (8000 psi) and temperatures of 427°C and 538°C. Assume that the stress exponent n is inde-

pendent of temperature. (b) Estimate $\dot{\epsilon}_s$ at 649°C (922 K).

- 9.54*** Steady-state creep rate data are given below for nickel at 1000°C (1273 K):

| $\dot{\epsilon}_s$ (s^{-1}) | σ [MPa (psi)] |
|---------------------------------|----------------------|
| 10^{-4} | 15 (2175) |
| 10^{-6} | 4.5 (650) |

If it is known that the activation energy for creep is 272,000 J/mol, compute the steady-state creep rate at a temperature of 850°C (1123 K) and a stress level of 25 MPa (3625 psi).

- 9.55*** Steady-state creep data taken for a stainless steel at a stress level of 70 MPa (10,000 psi) are given as follows:

| $\dot{\epsilon}_s$ (s^{-1}) | T (K) |
|---------------------------------|---------|
| 1×10^{-5} | 977 |
| 2.5×10^{-3} | 1089 |

If it is known that the value of the stress exponent n for this alloy is 7.0, compute the steady-state creep rate at 1250 K and a stress level of 50 MPa (7250 psi).

- 9.56** Cite three metallurgical/processing techniques that are employed to enhance the creep resistance of metal alloys.

Design Problems

- 9.D1*** Consider a flat plate of width 90 mm (3.5 in.) that contains a centrally positioned, through-thickness crack (Figure 9.12) of length (i.e., $2a$) 20 mm (0.8 in.). Determine the minimum plane strain fracture toughness necessary to ensure that fracture will not occur for a design stress of 375 MPa (54,400 psi). The $\pi a/W$ ratio is in radians.
- 9.D2*** A flat plate of some metal alloy contains a centrally positioned, through-thickness crack (Figure 9.12). Determine the critical crack length if the plane strain fracture toughness of the alloy is 38 MPa \sqrt{m} (34.6 ksi $\sqrt{in.}$), the plate width is 50 mm (2 in.), and the design stress is 300 MPa (43,500 psi). The $\pi a/W$ ratio is in radians.
- 9.D3*** Consider a steel plate having a through-thickness edge crack similar to that shown

in Figure 9.13a. If it is known that the minimum crack length subject to detection is 2 mm (0.08 in.), determine the minimum allowable plate width assuming a plane strain fracture toughness of $80 \text{ MPa}\sqrt{\text{m}}$ ($72.8 \text{ ksi}\sqrt{\text{in.}}$), a yield strength of 825 MPa (125,000 psi), and that the plate is to be loaded to one half of its yield strength.

- 9.D4*** Consider a steel plate having a through-thickness edge crack similar to that shown in Figure 9.13a; the plate width (W) is 75 mm (3 in.), and its thickness (B) is 12.0 mm (0.50 in.). Furthermore, plane strain fracture toughness and yield strength values for this material are $80 \text{ MPa}\sqrt{\text{m}}$ ($72.8 \text{ ksi}\sqrt{\text{in.}}$) and 1200 MPa (175,000 psi), respectively. If the plate is to be loaded to a stress of 300 MPa (43,500 psi), would you expect failure to occur if the crack length a is 15 mm (0.60 in.)? Why or why not?
- 9.D5*** A small and thin flat plate of a brittle material having a through-thickness surface crack is to be loaded in the manner of Figure 9.13c; the K_{Ic} value for this material is $0.45 \text{ MPa}\sqrt{\text{m}}$ ($0.41 \text{ ksi}\sqrt{\text{in.}}$). For a crack length of 0.25 mm (0.01 in.), determine the maximum load that may be applied without failure for $B = 4 \text{ mm}$ (0.16 in.), $S = 8 \text{ mm}$ (0.31 in.), and $W = 1 \text{ mm}$ (0.04 in.). Assume that the crack is located at the $S/2$ position.
- 9.D6** (a) For the thin-walled spherical tank discussed in Design Example 9.1, on the basis of critical crack size criterion [as addressed in part (a)], rank the following polymers from longest to shortest critical crack length: nylon 6,6 (50% relative humidity), polycarbonate, polyethylene terephthalate, and polymethyl methacrylate. Comment on the magnitude range of the computed values used in the ranking relative to those tabulated for metal alloys as provided in Table 9.2. For these computations, use data contained in Tables B.4 and B.5 in Appendix B.
- (b) Now rank these same four polymers relative to maximum allowable pressure according to the leak-before-break criterion, as described in the (b) portion of Design Example 9.1. As above, comment on these values in relation to those for the metal alloys that are tabulated in Table 9.3.
- 9.D7*** Consider a flat plate of some metal alloy that is to be exposed to repeated tensile-compressive cycling in which the mean stress is 25 MPa. If the initial and critical surface crack lengths are 0.15 and 4.5 mm, respectively, and the values of m and A are 3.5 and 2×10^{-14} , respectively (for $\Delta\sigma$ in MPa and a in m), estimate the maximum tensile stress to yield a fatigue life of 2.5×10^7 cycles. Assume the parameter Y has a value of 1.4, which is independent of crack length.
- 9.D8*** Consider a large, flat plate of a titanium alloy which is to be exposed to reversed tensile-compressive cycles of stress amplitude 100 MPa. If initially the length of the largest surface crack in this specimen is 0.30 mm and the plane strain fracture toughness is $55 \text{ MPa}\sqrt{\text{m}}$, whereas the values of m and A are 3.0 and 2×10^{-11} , respectively (for $\Delta\sigma$ in MPa and a in m), estimate the fatigue life of this plate. Assume that the parameter Y has a value of 1.45 which is independent of crack length.
- 9.D9*** Consider a metal component that is exposed to cyclic tensile-compressive stresses. If the fatigue lifetime must be a minimum of 1×10^7 cycles and it is known that the maximum initial surface crack length is 0.01 in. and the maximum tensile stress is 15,000 psi, compute the critical surface crack length. Assume that Y is independent of crack length and has a value of 1.75, and that m and A have values of 2.5 and 1.5×10^{-18} , respectively, for $\Delta\sigma$ and a in units of psi and in., respectively.
- 9.D10*** Consider a thin metal plate 20 mm wide which contains a centrally positioned, through-thickness crack in the manner shown in Figure 9.12. This plate is to be exposed to reversed tensile-compressive cycles of stress amplitude 125 MPa. If the initial and critical crack lengths are 0.20 and 8.0 mm, respectively, and the values of m and A are 4 and 5×10^{-12} , respectively (for $\Delta\sigma$ in MPa and a in m), estimate the fatigue life of this plate.

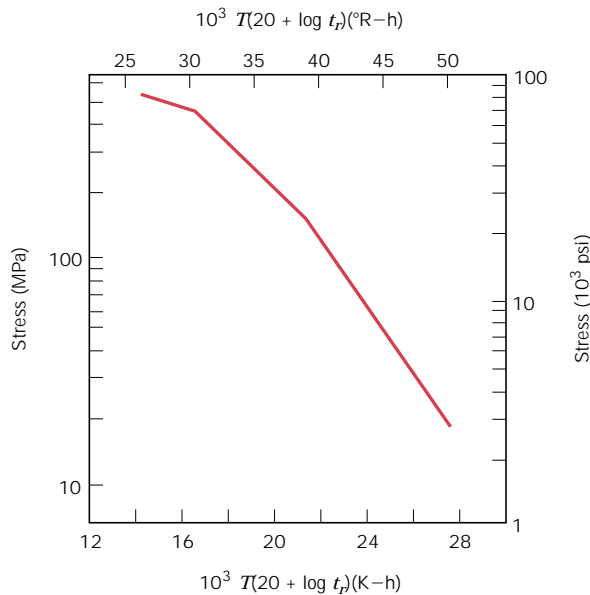


FIGURE 9.47 Logarithm stress versus the Larson–Miller parameter for an 18-8 Mo stainless steel. (From F. R. Larson and J. Miller, *Trans. ASME*, **74**, 765, 1952. Reprinted by permission of ASME.)

- 9.D11*** For an edge crack in a plate of finite width (Figure 9.13a), Y is a function of the crack length–specimen width ratio as



$$Y = \frac{1.1 \left(1 - \frac{0.2a}{W}\right)}{\left(1 - \frac{a}{W}\right)^{3/2}} \quad (9.36)$$

Now consider a 60 mm wide plate that is exposed to cyclic tensile-compressive stresses (reversed stress cycle) for which $\sigma_{\min} = -135$ MPa. Estimate the fatigue life of this plate if the initial and critical crack lengths are 5 mm and 12 mm, respectively. Assume values of 3.5 and 1.5×10^{-12} for the m and A parameters, respectively, for σ in units of megapascals and a in meters.

- 9.D12*** The spherical tank shown in Figure 9.15 is alternately pressurized and depressurized between atmospheric pressure and a positive pressure p ; thus, fatigue failure is a possibility. Utilizing Equation 9.31, derive an expression for the fatigue life N_f in

terms of p , the tank radius r and thickness t , and other parameters subject to the following assumptions: Y is independent of crack length, $m \neq 2$, and the original and critical crack lengths are variable parameters.

- 9.D13*** An S-590 iron component (Figure 9.44) must have a creep rupture lifetime of at least 100 days at 500°C (773 K). Compute the maximum allowable stress level.
- 9.D14*** Consider an S-590 iron component (Figure 9.44) that is subjected to a stress of 200 MPa (29,000 psi). At what temperature will the rupture lifetime be 500 h?
- 9.D15*** For an 18-8 Mo stainless steel (Figure 9.47), predict the time to rupture for a component that is subjected to a stress of 80 MPa (11,600 psi) at 700°C (973 K).
- 9.D16*** Consider an 18-8 Mo stainless steel component (Figure 9.47) that is exposed to a temperature of 500°C (773 K). What is the maximum allowable stress level for a rupture lifetime of 5 years? 20 years?